Ocean Engineering 302 (2024) 117661

Contents lists available at ScienceDirect

Ocean Engineering

journal homepage: www.elsevier.com/locate/oceaneng

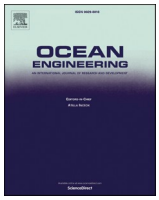

Research paper

The future of the Portuguese (SW Europe) most vulnerable coastal areas under climate change – Part I: Performance evaluation and shoreline evolution from a downscaled bias corrected wave climate ensemble

Gil Lemos [a,*], Ivana Bosnic [b], Carlos Antunes [a], Michalis Vousdoukas [c], Lorenzo Mentaschi [d], Pedro M.M. Soares [a]

[a] Universidade de Lisboa, Faculdade de Ciências, Instituto Dom Luiz, Lisboa, Portugal
[b] HAEDES, Portugal
[c] Department of Marine Sciences, University of the Aegean, University Hill, 81100, Mitilene, Greece
[d] University of Bologna: Bologna, Emilia-Romagna, Italy

ARTICLE INFO

Keywords:
Climate change
Coastal areas
Performance evaluation
Climate projections
Shoreline evolution

ABSTRACT

Some of the most disruptive effects of climate change are projected to be felt along the coastlines. The combined effects of future changes in water levels and wave climate along coastal areas constitute one of the most serious threats to their sustainable evolution, compromising critical infrastructures, resources, ecosystems, and communities. Understanding long-term changes in coastal areas remains challenging, however, due to their multivariate and multi-time-and-space-scale nature. In this study, we propose an innovative methodology for a complete vulnerability assessment of sandy low-lying coastal areas, based on dynamic, ensemble-based projections from the Coupled Model Intercomparison Project phase 5 (CMIP5). In the current Part I study, the effects of sea level rise (SLR) and nearshore wave climate changes on future shoreline evolution are assessed at five key-locations along the Portuguese coastline. Longshore sediment transport (LST) projections are computed, and sedimentary imbalances are quantified. Overall, robust shoreline retreat of up to 300 m is projected, especially along the Portuguese northern and central coastal areas, with continued erosion driven mainly by sediment imbalance and SLR. The projected decrease in future nearshore wave energy is responsible for a slight alleviation in erosion trends, up to 6.33%, whereas the increase of northerly incoming waves is expected to lead to northward beach rotations along western Mainland Portugal. The resulting shoreline evolution, responsible for the loss of up to 0.786 km^2 of dry land by 2100 along the 14 km of analysed coastline, is projected to threaten several Portuguese urban areas, calling for the implementation of adequate coastal management and adaptation plans, to reduce the impacts of climate change on population, infrastructures, livelihood, and ecosystems.

1. Introduction

Coastal areas are amongst the most vulnerable regions to climate change, comprising important populational centres and economically relevant hubs (IPCC, 2014; 2022; Hallegatte et al. 2013; Hinkel et al. 2014; Kulp and Strauss, 2020; Feyen et al., 2020). The portion of total population living in coastal areas has rapidly increased in the last decades (Neumann et al., 2015; Rentschler et al., 2023), being estimated that at least 10% of the current world's population lives in coastal areas less than 10 m above sea-level (McGranahan et al., 2007; Reimann et al., 2023).

Rising sea levels (Storlazzi et al., 2018), together with the effects of tides, storm surges (Camelo et al., 2020) and extreme waves (Senechal et al., 2011) are considered key-drivers of coastal hazards, threatening coastal infrastructures, ecosystems, and communities. The increase in human pressure along the global coastlines (Jones and O'Neill, 2016) calls for reliable, long-term coastal vulnerability assessments, needed for effective coastal management, sustainable development, adaptation, and impact mitigation strategies. In this context, the National Roadmap for Adaptation XXI – Portuguese Territorial Climate Change Vulnerability Assessment for XXI Century (RNA2100) project is currently underway, with the goal of supporting public policy exercises of adaptation

* Corresponding author.
E-mail address: grlemos@ciencias.ulisboa.pt (G. Lemos).

https://doi.org/10.1016/j.oceaneng.2024.117661
Received 19 October 2023; Received in revised form 16 February 2024; Accepted 24 March 2024
Available online 4 April 2024

to climate change, at different levels of territorial intervention in Portugal. RNA2100's main aims include the characterization of climate change physical and socioeconomic impacts on the Portuguese most vulnerable domains, the assessment of financial costs and needs, and the implementation of a National Spatial Planning Policy Programme (Soares and Lima, 2022; Soares et al., 2023a, 2023b; Lima et al., 2023a, 2023b).

The Portuguese coastline extends for about 980 km, and most of the Portuguese populational centres are located at the coast. According to Rocha et al. (2020), 14% of the national population lives within 2 km of the sea. In a recent update of the national census (CENSOS 2021), it was shown that the population living in the Lisboa and Algarve regions increased by 1.7% and 3.7% relative to 2011, adding further pressure on the Portuguese coastal areas. Overall, the Portuguese coastline is composed of sandy beaches, dunes, sandy rocky and soft cliffs, interspersed by river mouths, estuaries, lagoon systems, barrier islands and urbanized areas with maritime ports, sea walls, breakwaters, marginal roads and housing lots. Such a complex coastal setting poses enormous challenges in the definition of accurate and consistent coastal vulnerability and risk assessment methodologies.

Modelling long-term shoreline evolution and extreme coastal flooding is a challenging task, mainly due to the computational cost of dynamic modelling efforts and the high number of variables involved (Ranasinghe, 2016; Toimil et al., 2020). Therefore, many studies focus solely on the effects of SLR, neglecting or considering the remaining variables stationary (*e.g.*, Athanasiou et al., 2020; Le Cozannet et al., 2019). Methodologies often overlook details such as model validation in local context, performance assessment of forcing (GCM or GCM-driven) variables, through comparison with local observations, the implementation of bias correction techniques, if necessary, or even the effects of wave shoaling, crucial for accurate assessments at the shore.

Pervasive wave action along a sandy shoreline modulates its sedimentary balance with the establishment of longshore currents which, in the absence of human action, are responsible for both short- and long-term free shoreline evolution. While the evolution of the shoreline, depending primarily on waves and coastline orientation, may consist of a retreat or accretion depending on their mean wave direction (*MWD*), the effect of SLR promotes a long-term consistent retreat, forcing the equilibrium profile landward to preserve its shape relative to the sea level (Vousdoukas et al., 2020). At a global scale, Luijendijk et al. (2018) showed that, since 1984, 24% of the world's sandy beaches are eroding at rates exceeding 0.5 m/year, while 48% are stable and 28% are accreting. Mentaschi et al. (2018), considering erosion in estuaries as well, found a global eroded area of 28.000 km^2 in 32 years, twice the accretion during the same period. Although the global distribution of eroding and accreting sandy beaches is irregular, greatly depending on the local wave climate characteristics and shoreline orientation, Portugal has been shown to be in an area of high erosive trends (Pinto et al., 2020). In fact, erosion in Portugal has been thoroughly studied over the last decades (*e.g.*, Duarte Santos et al., 2014; Pinto, 2016; Lira et al., 2016; Ferreira et al., 2020), being determined that from 1958 to 2021, the total area lost to the sea, at national scale, amounted to 13.5 km^2, with 45% of the Portuguese low sandy beaches currently under erosion (Pinto et al., 2020).

The continued rising sea levels along Portuguese coastlines (Antunes, 2014), associated with the present scenario of coastal sedimentary imbalance, could result in unprecedented coastal flooding, if no additional coastal protection and risk-reduction or adaptation measures are implemented (Duarte Santos et al., 2014). In the context of an increasing need for accurate physical and socioeconomic coastal vulnerability assessments, and incorporated in the RNA2100 project, this study proposes an innovative methodology to deal with the multivariate challenges of an accurate coastal vulnerability assessment for Portugal, considering the effects of SLR, tides, storm surge and waves along the coastal areas, in terms of future shoreline evolution and extreme coastal flooding, through high-resolution hydro- and morpho-dynamic modelling. Ensemble-based projections are used to drive a collection of dynamic models, providing baseline results for a complete, national-scale coastal vulnerability assessment, based on a composed coastal vulnerability index. This study further aims at establishing the grounds for translating physical impacts into social and economic ones, as well as adaptation and impact mitigation measures. The complete assessment is carried out in two parts and published in companion papers. Here, in Part I, the datasets are presented, the overall methodology is outlined and detailed, and future high-resolution shoreline evolution projections are presented along five representative coastal domains along the Portuguese coastline, based on CMIP5 multi-model ensembles of SLR and nearshore wave climate projections, under the Radiative Concentration Pathways (RCPs) 4.5 and 8.5 (Riahi et al., 2011). Our goal in Part I is to present, for the first time, coherent ensemble-based shoreline projections along highly vulnerable areas of the Portuguese coastline, towards the end of the 21st century. The five key-locations, chosen according to their increased vulnerability and risk to the effects of climate change (*i.e.*, strong sedimentary imbalance, extreme storminess, SLR and proximity to urbanized areas), constitute testbeds for the complete application of the methodology (at a national scale), generating baseline results. In Part II, the future projected shorelines are used to modify the present-day digital terrain models (DTMs) using an innovative parametric coastal retreat method. Nearshore bias-corrected extreme total water level (TWL) projections are built, using a probabilistic approach, for an accurate assessment of future extreme coastal flooding impacts. Finally, the ensemble-based future projected flooded areas determined, highlighting the effects on coastal urbanized zones. The overall assessment carried out in Parts I and II ultimately aims at providing the necessary data to map coastal vulnerability along the entire coast of Mainland Portugal, translating the local dynamic modelling results into a composed coastal vulnerability index, enabling the identification of the potential risk zones.

This article is organized as follows: in section 2, the study areas are defined, along with the five key-locations where the high-resolution dynamic modelling is conducted. The datasets used are also defined, and the detailed methodology of each sub-task is presented. A thorough description of the results is offered in section 3. A discussion of the results and the main conclusions drawn from Part I are provided in section 4.

2. Data and methods

2.1. Study areas

The Portuguese coastline includes extensive sandy beaches backed by dunes and cliffs, bays, estuaries, lagoons, natural and artificialized inlets and barrier islands, hosting major and highly strategic political, economic, industrial and commercial structures, as well as densely urbanized areas. After careful consideration of the coastal sectors, five specific key-locations were selected, in a coordinated manner with the Portuguese Environmental Agency (APA; Pinto et al., 2022). Enhanced current erosive trends and imminent overtopping and coastal flooding, together with the proximity of population centres to the coast focused the need for local modelling efforts. The five selected key-locations reflect well the geomorphological heterogeneities of the Portuguese low-lying sandy coastline, benefiting from large field observational datasets, as well as from the proximity to buoys, for the characterization of the sea states. The selected key-locations are: Ofir, Costa Nova, Cova Gala, Costa da Caparica and Praia de Faro (Fig. 1).

Ofir is located in the northwestern coast of Portugal, in a particularly vulnerable area due to intensive human occupation along the coastal fringe. This coastal stretch shows some of the highest historical erosion trends at a national scale (Lira et al., 2016). Consistently decreasing beach widths motivated the construction of coastal defence structures between the 1970s and the 1990s (Veloso-Gomes et al., 2004). During the winter season, waves are dominant from the W-NW (270-315°),

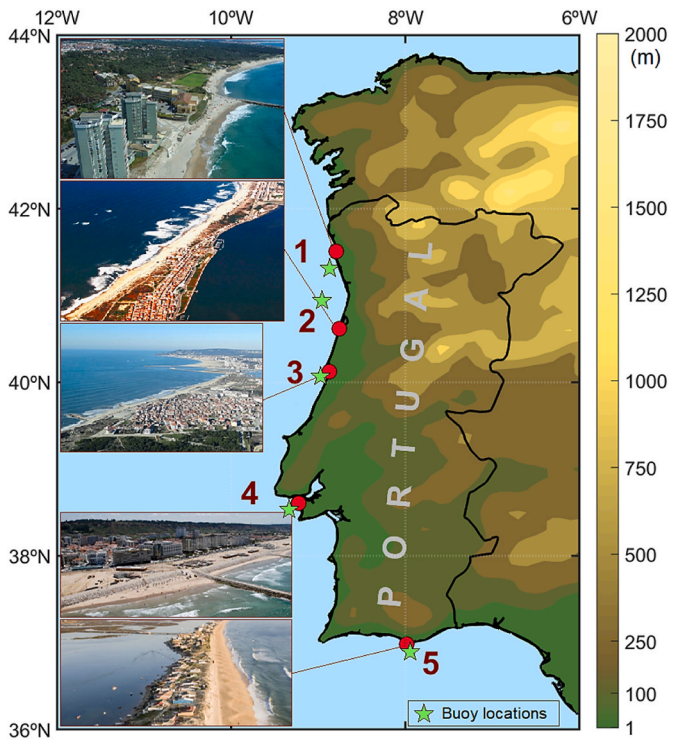

Fig. 1. Key-locations along Mainland Portugal's coastline: 1) Ofir, 2) Costa Nova, 3) Cova Gala, 4) Costa da Caparica and 5) Praia de Faro. *In-situ* observational instruments (the reader is referred to section 2.5.) are marked as green stars.

often exceeding significant wave heights (H_S) of 6 m (Semedo et al., 2011; Lemos et al., 2019, 2020, 2020b, 2021a).

Costa Nova is a sector of the central Portuguese western coast, located south of Ria de Aveiro mouth. This sandy barrier protects the southern arm of the Ria, with extensive agricultural and urbanized occupation. The dune system of Costa Nova is becoming more exposed to wave action, with increasing erosion due to widespread sedimentary deficit (Fernández-Fernández et al., 2019). According to Vicente and Clímaco (2015), from 1958 to 2015 the shoreline between Costa Nova and Vagueira has retreated approximately 400 m, significantly affecting the coastal communities. While recent assessments suggest that the areas North of the Ria de Aveiro mouth may be experiencing sedimentary accretion, due to the new configuration of the jetty (Coelho et al., 2021a, b), in the southern sectors (including Costa Nova), a dominant erosive trend is still detectable (Fernández-Fernández et al., 2019; Bernardes et al., 2020; Pinto et al., 2022). Climatologically, similarly to the Ofir key-location, waves are dominant from the W-NW (270-315°) sectors, with annual H_S maxima above 6 m.

Cova Gala is located in the central Portuguese western coast, South of Figueira da Foz. Erosion trends in this sector have been shown to be increasing (Oliveira and Brito, 2015; Nunes and Cordeiro, 2013), with 82% of the coastal stretch that includes Cova Gala experiencing coastal retreat from 2018 to 2021, 66% of it classified as under severe or extreme erosion (corresponding to average annual rates of −4 m/year; Pinto et al., 2022). Similarly to the previous locations, waves are dominant from the W-NW (270-315°) and often exceed H_S values of 6 m.

Costa da Caparica is located South of the Tagus River mouth and is a well-known and densely occupied urban area and touristic resort, benefiting from its proximity to Lisbon. Major coastal planning efforts have been put in place over time to mitigate and adapt to the local strong coastal erosion trends. Between 1959 and 1963, three groynes and a longshore seawall were placed to attenuate erosion on the northernmost part of the Costa da Caparica sector. Between 1968 and 1971, these structures were expanded, and seven more groynes were built (IHRH, 2003). Between 2007 and 2019, several beach nourishment interventions were performed at Costa da Caparica, totalizing 4.5×10^6 m^3 (Pinto et al., 2007, 2015; Veloso-Gomes et al., 2009). Nevertheless, overtopping is still common during winter, especially under stormy weather or extreme swell events. Waves are dominant from the W (270°), with H_S values frequently exceeding 4 m during winter, and 6 m about once every two years.

Praia de Faro is inserted in the Ria Formosa natural park (a shallow meso-tidal coastal lagoon protected by 2 peninsulas and 5 barrier islands), in the Algarve region, close to the city of Faro. The location is home to a small community of fishermen, and it is used as a recreational area for tourists and locals. It is composed of a narrow dune strip between the Atlantic Ocean and Ria Formosa, which is mainly affected by long-term erosion driven by changes in the sea level, storms and human interventions that modify the natural configuration of the area, such as the use of summer houses and trampling paths, crossing the dune (Domingues et al., 2021). Waves are dominant from the SW-W (225-270°) and although generally detaining low to moderate energy, relatively intense storms (with H_S values higher than 3 m) occur during winter, mostly from SE (135°).

2.2. GCM-driven wave climate simulations

A 6-member ensemble of wave climate simulations and projections is used in this study, produced within the context of the Large Scale Integrated Sea-Level and Coastal Assessment Tool (LISCoAsT) project, and presented in Vousdoukas et al. (2017) and Mentaschi et al. (2017). The third-generation spectral wave model WaveWatchIII (WW3; Tolman, 2002) was forced with near-surface winds from 6 GCMs, producing a 6-member multi-model ensemble, spanning from 1971 to 2100, under the RCP4.5 and RCP8.5 scenarios. WW3 was set-up using the ST4 parameterization (Ardhuin et al., 2010), shown to improve the evolution of waves for long distances, with a positive impact on the model performance at a global scale (Rascle and Ardhuin, 2013). This characteristic is particularly important for a more accurate description of the wave climate along the Portuguese coastlines, given that extreme wave storms are mostly composed of relatively long swells (generated in the North Atlantic). The horizontal resolution of the 6-member ensemble for the southwestern Europe domain is 0.5°. The wave parameters considered here include the H_S, the peak wave period (T_p) and the mean wave direction (*MWD*). Further details can be found in Table 1.

2.3. Sea level rise

Since pre-industrial times, it is estimated that the global sea level has already risen approximately 20 cm (Nerem et al., 2010; Church and White, 2011; Hay et al., 2015; Sweet et al., 2017, 2022; IPCC et al., 2022). Although there is a very low rate of regional uplifting along the Portuguese coastline (Cabral, 1995; Figueiredo et al., 2014), local SLR measurements from the Cascais tide gauge (near Lisbon) reveal values in line with the global mean (Antunes et al., 2019), showing a progressive response to global warming.

The SLR projections used here were obtained from CMIP5 GCMs outputs, following Church, 2013. The complete SLR dataset includes projections from 21 GCMs for the RCP4.5 and RCP8.5 future scenarios. The mean SLR projections are extracted from each ensemble, at the closest grid-point to each key-location.

2.4. The ERA5 reanalysis

The ERA5 reanalysis (Hersbach et al., 2020) provides a detailed record of the global atmosphere, land surface and ocean waves from 1940 onwards. The ERA5 includes improvements in model physics, core dynamics and data assimilation, when compared with its predecessor, the ERA-Interim (Dee et al., 2011), besides a considerable increase in horizontal, vertical and time resolutions. The ERA5 global grid has a

Table 1
Summary of the GCMs used for the historical and future experiments under RCP4.5 and RCP8.5. For the different climate scenarios, the symbol ✓ indicates the availability of SLR and wave parameters, while the SLR and W indicate the availability of solely SLR and wave parameters, respectively. The symbol — indicates data unavailability.

GCM	Institute (country)	Hist.	RCP4.5	RCP8.5
ACCESS1.0	Commonwealth Scientific and Industrial Research Organisation – Bureau of Meteorology (Australia)	W	✓	✓
ACCESS1.3	Commonwealth Scientific and Industrial Research Organisation – Bureau of Meteorology (Australia)	W	W	W
BCC-CSM1.1	Beijing Climate Centre (China)	–	SLR	SLR
CanESM2	Canadian Centre for Climate Modelling and Analysis (Canada)	–	SLR	SLR
CNRM-CM5	Centre National de Recherches Météorologiques (France)	–	SLR	SLR
CSIRO-Mk3.6.0	Commonwealth Scientific and Industrial Research Organisation - Queensland Climate Change Centre of Excellence (Australia)	W	✓	✓
EC-EARTH	EC-EARTH consortium	W	W	W
GFDL-ESM2G	NOAA Geophysical Fluid Dynamics Laboratory (USA)	W	✓	✓
GFDL-ESM2M	NOAA Geophysical Fluid Dynamics Laboratory (USA)	✓	✓	✓
GISS-E2-R	NOAA Geophysical Fluid Dynamics Laboratory (USA)	–	SLR	SLR
HadGEM2-CC	Met Office Hadley Centre (UK)	–	SLR	SLR
HadGEM2-ES	Met Office Hadley Centre (UK)	SLR	SLR	SLR
IPSL-CM5A-LR	Institut Pierre-Simon Laplace (France)	SLR	SLR	SLR
IPSL-CM5A-MR	Institut Pierre-Simon Laplace (France)	–	SLR	SLR
INMCM4	Institute for Numerical Mathematics (Russia)	–	SLR	SLR
MIROC-ESM	Agency for Marine-Earth Science and Technology (Japan)	–	SLR	SLR
MIROC-ESM-CHEM	Agency for Marine-Earth Science and Technology (Japan)	–	SLR	SLR
MIROC5	Agency for Marine-Earth Science and Technology (Japan)	SLR	SLR	SLR
MPI-ESM-LR	Max Planck Institute (Germany)	–	SLR	SLR
MPI-ESM-MR	Max Planck Institute (Germany)	–	SLR	SLR
MRI-CGCM3	Meteorological Research Institute (Japan)	–	SLR	SLR
NorESM1-M	University Corporation for Atmospheric Research (USA)	–	SLR	SLR
NorESM1-ME	University Corporation for Atmospheric Research (USA)	–	SLR	SLR

horizontal resolution of 0.25° (31 km) for the atmosphere and 0.36° (40 km) for the waves, with 1-hourly output time resolution. The ERA5 is produced using the ECMWF Integrated Forecast System (IFS) Cy41r2 (ECMWF, 2016) and updated in almost real-time.

Regarding ocean waves, hourly assimilation of altimeter wave data is carried out in ERA5 from 1991 onwards (using data from most missions), through the 4-dimensional variational (4D-Var) analysis system and the Optimum Interpolation scheme to ensure hourly updates of the wave fields. Therefore, ERA5 data are fully synchronous in time with real-world observations. Here, wave data from the ERA5, comprising H_S, mean wave period (T_m), T_p and *MWD*, are used as a long-term continuous reference dataset. The original time-series, at the closest offshore grid-point are propagated towards the *in-situ* buoy locations using the SWAN wave model (the reader is referred to section 2.6.1.). These are locally corrected using bias correction methods, being then propagated again towards the shore.

2.5. In-situ buoy data

In-situ buoy observations are used at the five key-locations to assess the performance of the ERA5 reanalysis in depicting the H_S, T_m, T_p and *MWD* climate, considering the available observational periods. Despite being a reanalysis, built using advanced assimilation methods based on *in-situ* observations and satellite altimetry measurements, the ERA5 is not able to capture local phenomena as accurately as the buoys (Bidlot et al., 2019; Wang and Wang, 2022). Therefore, to promote a more correct representation of local features, such as changes in *MWD* driven by nearshore bathymetry, *in-situ* wave observations are used to correct the ERA5, using a quantile mapping bias correction methodology (the reader is referred to section 2.6.1).

Five buoys are used in the present assessment. These correspond to the Leixões buoy (IH), Costa Nova buoy (RAIA project; Allen-Perkins et al., 2007), Figueira da Foz buoy (IH), Lisbon buoy ("Administação do Porto de Lisboa"; APL), and Praia de Faro buoy (IH). The geographical location and period covered by each buoy can be found in Table 2.

2.6. Methodology

2.6.1. Wave propagation and bias correction

Modelling often exhibits systematic errors (biases) when compared to reference datasets, arising from simplified physics or numerical parameterizations within the models (Rocheta et al., 2017; Maraun et al., 2017, 2019; Gutiérrez et al., 2019; Soares et al., 2019). Attempting to correct these errors, bias correction methodologies have become a standard procedure in climate change studies. These post-processing tools aim to improve the model agreement with reference data (*e.g.*, observations, reanalyses, hindcasts), assuming that the bias behaviour does not change in time (*i.e.*, the bias remains stationary between historical simulations and future projections; Haerter et al., 2011). The main purpose of bias correction is to promote greater consistency between the reference and simulated climates.

Here, two bias correction methods are applied to the wave climate simulations and projections, namely the Empirical Gumbel Quantile Mapping (EGQM) and the Empirical Quantile Mapping (EQM), following Lemos et al. (2020a, 2020b), to better characterize the local wave climate features at each of the five key-locations. On a first stage, the entire ERA5 reanalysed period (1971–2020), propagated from offshore to the buoy locations, is corrected, for H_S, T_m, T_p (EGQM) and *MWD* (EQM), using observed information from each of the five buoys. The *MWD* is corrected using a simplified version of the EGQM, the EQM, given its circular behaviour. *MWD* data were transformed into zonal (u) and meridional (v) components, being each one corrected individually, and finally used to reconstruct the bias corrected *MWD* parameter.

The propagation of the original GCM-driven wave fields (section 2.2. And Table 1) from the offshore grid-points to the *in-situ* and coastal locations is conducted using the SWAN wave model (Booij et al., 1999), designed specifically for coastal waters, lakes and estuaries. The model is based on the wave action balance equation with sources and sinks.

Table 2
Details regarding the *in-situ* observational instruments (buoys).

Buoy	Institution	Lat (°)	Lon (°)	Depth (m)	Period
Leixões	IH	41.32°N	8.98°W	83	28-07-1993 – 05-04-2018
Costa Nova	RAIA	41.15°N	9.58°W	1684	23-10-2010 – 19-03-2020
Figueira da Foz	IH	40.13°N	8.90°W	13	06-07-1984 – 05-02-1996
Lisboa	APL	38.62°N	9.38°W	22	31-07-2005 – 27-06-2011
Faro	IH	36.90°N	7.88°W	93	19-03-2009 – 05-04-2018

SWAN version 41.31 is used here to propagate the offshore GCM-driven waves to nearshore, between 10 m and 20 m depth, allowing to consider the effects of local bathymetry changes while approaching the coast using a high-resolution bathymetry dataset (EMODnet). The model is set up in the stationary mode, using a structured grid with a horizontal resolution of 250 m, extending offshore by 3 km. Such configuration is considered reasonable to depict the transformation of the most energetic wave events, responsible for the greatest changes in shoreline configuration. Finally, the ShorelineS (Roelvink et al., 2020) is forced with the propagated and bias corrected nearshore waves.

The propagation and correction schemes are schematized in Fig. 2. In summary, first, the ERA5 data is propagated from the offshore grid-point to the closest *in-situ* location. The ERA5 is then bias corrected and finally propagated nearshore, to depths between 10 m and 20 m. Simultaneously, the GCM-driven wave climate simulations and projections are propagated from their original offshore grid-points towards the same final location, being then bias corrected using the corrected ERA5 data.

2.6.2. The ShorelineS model

Currently available shoreline evolution models vary greatly in their complexity, computational demands, and stable simulation horizon (Roelvink, 2011; Ranasinghe, 2020; Toimil et al., 2020; Hunt et al., 2023). Two main model classifications are commonly considered: physics-based models and process-based models. While physics-based models can numerically resolve the majority the complex morpho- and hydro-dynamic processes through equations of mass and momentum conservation, process-based (or reduced-complexity) ones rely on the parameterization of a limited number of dominant coastal processes, without explicitly resolving the underlying hydro-dynamic processes responsible for sediment transport (Vitousek et al., 2023). Recent studies have shown that physics-based models recommended to simulate the coastal morphological evolution from seasonal to decadal time scales, especially due to the inefficiency (low overall computational-cost-benefit ratio) of process-based models in multi-year coastal area applications (French et al., 2016; Sherwood et al., 2022). The (physics-based) Shoreline Simulation (ShorelineS) model (Roelvink et al., 2020) is a free-form coastline model capable of describing drastic coastal transformations based on relatively simple principles borrowed from general coastline theory (Pelnard-Considere, 1956). This open-source MATLAB-based model describes the coastline like a freely moving string of points for an arbitrary number of coastal sections (open/closed) that can interact with rocky parts and/or structures.

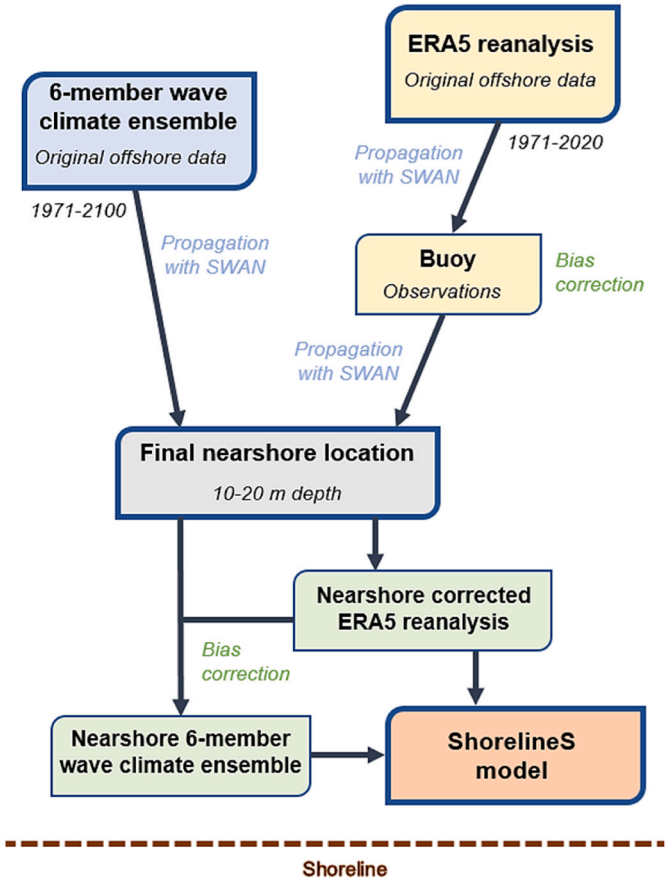

Fig. 2. Scheme for offshore wave propagation and bias correction. The large yellow box corresponds to a generic ERA5 offshore grid-point, propagated and corrected at buoy location, and the blue box to a generic offshore grid-point of the wave climate simulations and projections ensembles. Both the corrected ERA5 and ensembles are propagated to a final nearshore location, where the latter are corrected and finally used to force the ShorelineS model.

The ShorelineS model is employed here to simulate the shoreline evolution under the different scenarios, according to the associated future projected wave climates and SLR values. From the available sediment transport formulas in the model, CERC3 (U. S. Army Corps of Engineers, 1984) is considered, accounting for wave height at the breaking zone, and being computationally more efficient than, for instance, the Kamphuis (KAMP; Kamphuis, 1991) formula (which also required inputs such as beach slope and grain size, not available for all key-locations considered). Neumann boundary conditions are selected. The model is first calibrated and validated against shoreline observations, and its performance in simulating the evolution of the shoreline is evaluated using the bias corrected ERA5 wave data at the five key-locations, from 2008 to 2018 (timeframe with available high-resolution observations). The observed shorelines correspond to the berm heights obtained from the aerial photogrammetric survey provided by the Portuguese National Directorate-General for Territory (DGT), as well as from the COSMO programme developed by APA (at 1 m resolution). Then, each of the 6 individual members from the nearshore bias corrected ensemble of wave climate projections is used to force the ShorelineS model towards the end of the 21st century. Since shoreline evolution is a continuous process, the moment in time considered for the future projected 2041–2070 (2071–2100) time-slice is the year 2070 (2100), corresponding to the end of the time-slice. The final projected shoreline is the average of the 6 independent ensemble member projections, from the range of natural inter-member uncertainty. It should be noted that the ShorelineS version used in this work does not account for changes in the sea level during the simulation periods, as forcing is restricted to waves, and therefore, not allowing the direct inclusion of SLR and tide oscillations. Hence, the additional effects of SLR are included *a posteriori*, using Bruun's rule (Bruun, 1962, 1988), accounting for the available accommodation space at each location. Bruun's rule is a two-dimensional mass conservation principle describing the landward retreat of the shoreline (and the overall equilibrium profile) along sandy beaches in response to SLR. Despite widespread criticism (Cooper and Pilkey, 2004; Ranasinghe et al., 2012), Bruun's rule is currently the only computationally viable approach to determine long-term shoreline retreat due to SLR, being commonly used in scientific literature from local to global scales (Zhang et al., 2004; Hinkel et al., 2014; Udo and Takeda, 2017; Ritphring et al., 2018; Vousdoukas et al., 2020).

3. Results

3.1. Performance of the propagated-corrected wave climate simulations

As described in Fig. 2, the 6-member ensemble of wave climate simulations, spanning over the 1971–2000 historical period, was subjected to a propagation-correction scheme to consider both the wave transformation near the coast, as well as a correction of the systematic biases, using ERA5. Fig. 3 shows the wave field transformation for the historical 6-member ensemble (all members pulled together) at each of

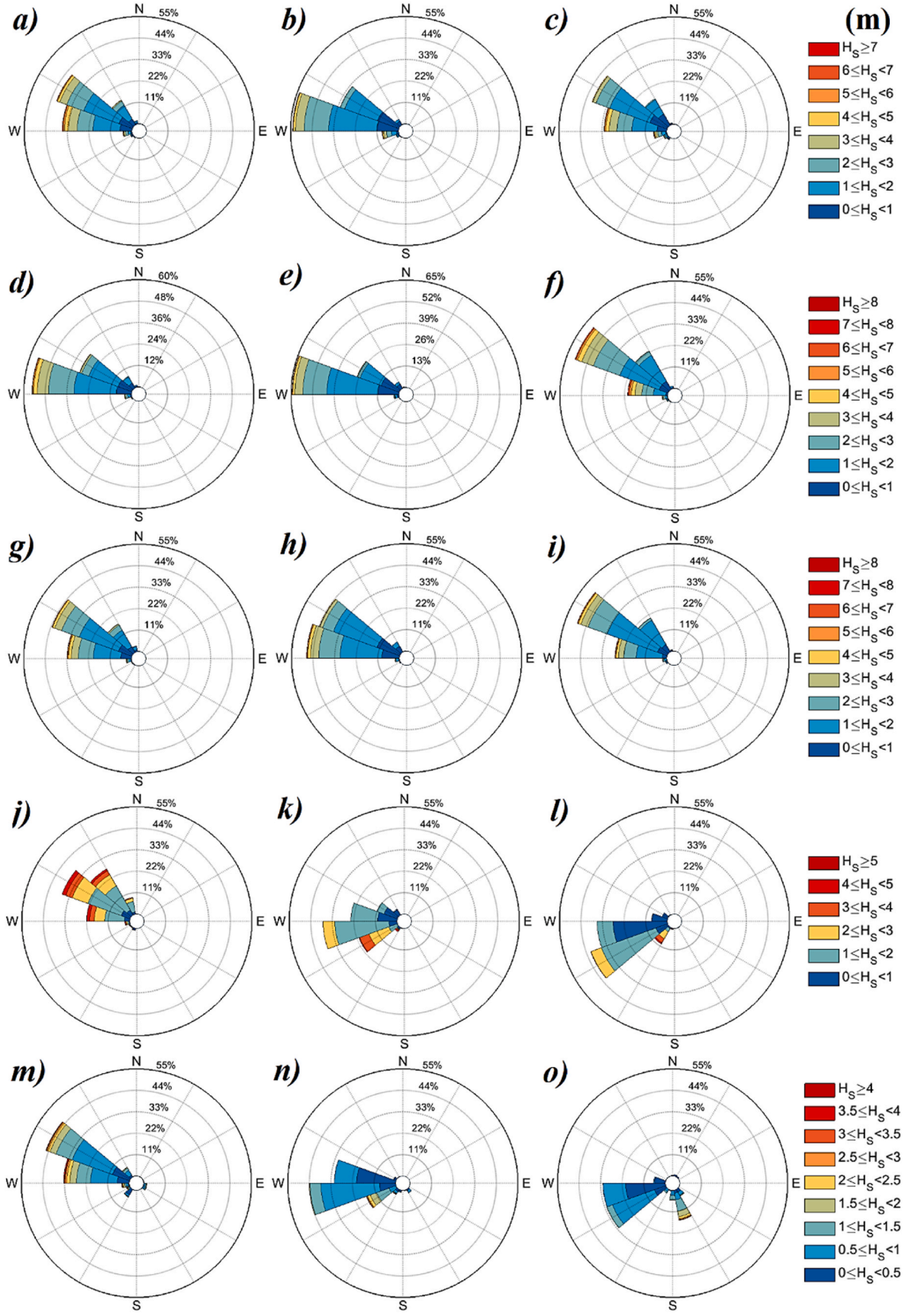

Fig. 3. Wave field transformation of the ensemble during present climate (1971–2000) using the propagation-correction methodology, at the (a–c) Ofir, (d–f) Costa Nova, (g–i) Cova Gala, (j–l) Costa da Caparica and m-o) Praia de Faro key-locations. Original ensemble wave fields (a,d,g,j,m – left), propagated ensemble wave fields (b,e,h,k,n – centre) and propagated-corrected ensemble wave fields (c,f,i,l,o – right).

the key-locations. Tables SM1 to SM5 in the SM detail the differences between the propagated-corrected historical ensembles frequencies of occurrence for each H_S and *MWD* bin, and ERA5. Overall, while the offshore ensemble (Fig. 3 – left) is able to capture the major directional characteristics of the coastal wave fields at the Ofir (Fig. 3a), Costa Nova (Fig. 3d) and Cova Gala (Fig. 3g), its performance is rather low at Caparica (Fig. 3j) and Praia de Faro (Fig. 3m), given their complex geographic and morphological contexts, which are not well represented by a global product. At the first three locations, upon propagation and correction, the northwesterly component is enhanced, especially at Costa Nova (Fig. 3f). Possibly due to local conditions, the highest H_S values at the coast occur there as well, surpassing 4 m during 7.74% of the historical period (Table SM2). At Praia de Faro, the coastal wave fields exhibit perhaps the most considerable change from their original offshore characteristics (Fig. 3m). Near the shore (Fig. 3o), while low waves (H_S below 1.5 m) are often from WSW (230°–270°; approximately 65% dominance), the highest H_S values are originated by waves from SSE (150°–170°), with a frequency of occurrence of 1.96% for values greater than 2 m (Table SM5).

Table 3 shows the overall performance of the nearshore propagated-corrected ensemble wave fields at the key-locations, in comparison with the coastal propagated-corrected-propagated nearshore ERA5 reference data, in terms of the joint frequency of occurrence of all waves for each *MWD* bin (values corresponding to the ones displayed in Fig. 3). Not surprisingly, at the coast, the overall ensemble's performance is better at the Ofir, Costa Nova and Cova Gala key-locations, with differences below 0.2% for all directional bins. At Costa da Caparica and Praia de Faro, the differences tend to be slightly greater, however, not exceeding 3.3% in both cases. While the corrected ensemble tends to underestimate the southwesterly components at Costa da Caparica and Praia de Faro, it overestimates the westerly ones. This feature was also apparent before the correction at the coast, being, nevertheless, smoothed after the procedure.

3.2. Future wave climate and SLR projections

The performance evaluation conducted for the historical propagated-corrected wave climate simulations at the five key-locations provided the necessary confidence in the ability of the ensemble to accurately simulate the local wave climatology and therefore provide a realistic climate change signal until 2100. Figs. SM1 to SM5 in the Supplementary Material (SM) describe the projected changes for each key-location's joint H_S and *MWD* fields (mean and 95% percentile values). Additionally, Tables SM6 to SM10 show the projected frequencies of occurrence for each H_S and *MWD* bins along the entire directional ranges. Table 4 provides a summary of Tables SM6 to SM10, considering all H_S values, and Table SM11 describes the projected changes in the ensemble mean and 95% percentile H_S values at each key-location.

The projected changes at Ofir (Table 4, and Fig. SM1 and Table SM6 in the SM) show an overall increase in the frequency of occurrence of lower H_S values (below 1 m), ranging between 1.4% and 3.3% considering both RCPs after 2041. For H_S values above 1 m, frequencies are projected to decrease by the same order of magnitude as mentioned, however these are shown to be greater up to the 3 m mark (between 0.6% and 1.4% for 1–2 m, and 0.6%–1.2% for 2–3 m). Events with H_S above 6 m are projected to decrease only marginally (from 0.47% down to 0.43% during 2071–2100 under RCP8.5). Regarding the mean and 95% percentile H_S associated with each *MWD* bin, differences are usually small, below 0.2 m, referring to projected increases (decreases) southwards (northwards) of 265° (W). Nevertheless, integrated projections point to overall projected decreases in H_S, down to −4.02% (−2.33%) for the mean (95% percentile) values (Table SM11). These are consistent with previous studies conducted for the eastern North Atlantic (*e.g.* Lemos et al., 2021a). Note, however, that extreme H_S values within the 230-240° range are projected to increase during 2071–2100 under RCP8.5, compatible with more severe storm events from the SW, possibly associated with higher-latitude tropical and/or post-tropical cyclones in a warmer climate by the end of the 21st century (Studholme et al., 2022).

For Costa Nova (Table 4, and Fig. SM2 and Table SM7 in the SM), the

Table 3
Near the coast H_S frequency of occurrence (FO) at each directional bin (20°) for the historical ensemble (H) and ERA5 (1971–2000). Absolute differences (biases): green below 1%, yellow between 1% and 2%, orange between 2% and 3%, dark orange between 3% and 4%, red between 4% and 5% and dark red above 5%.

Directions (°)	FO ERA5 Ofir (%)	FO H Ofir (%)	FO ERA5 Costa Nova (%)	FO H Costa Nova (%)	FO ERA5 Cova Gala (%)	FO H Cova Gala (%)	FO ERA5 Costa da Caparica (%)	FO H Costa da Caparica (%)	FO ERA5 Praia de Faro (%)	FO H Praia de Faro (%)
[350-10[	0.04	0.08	0.04	0.06	-	0.01	0.01	0.01	0.17	0.45
[10-30[	0.07	0.09	0.03	0.10	-	0.01	0.00	0.01	0.11	0.94
[30-50[	0.04	0.14	0.03	0.11	-	0.01	0.00	0.01	0.17	0.55
[50-70[	0.03	0.01	0.01	-	-	0.01	0.02	0.02	0.16	0.07
[70-90[	0.06	-	0.01	-	-	-	0.08	-	0.24	-
[90-110[	0.01	-	0.03	-	-	-	0.12	-	0.58	-
[110-130[	0.02	-	0.03	-	-	-	0.06	-	1.23	0.01
[130-150[	0.01	0.01	0.04	-	-	-	0.06	0.30	3.39	4.21
[150-170[	0.02	-	0.01	-	-	-	0.16	0.15	14.6	15.7
[170-190[	0.02	-	0.02	-	-	-	0.14	0.14	6.57	5.04
[190-210[	0.19	0.09	0.08	-	-	-	0.86	0.62	0.60	0.49
[210-230[	1.17	1.30	0.40	0.41	0.28	0.26	12.9	9.70	2.47	2.24
[230-250[	2.17	2.17	1.08	1.21	1.14	1.06	40.7	41.8	33.6	32.1
[250-270[	6.78	6.80	3.03	3.10	2.24	2.31	33.5	35.9	28.7	32.0
[270-290[	32.0	32.0	20.4	20.4	26.4	26.4	10.1	7.99	6.86	5.96
[290-310[	40.7	40.7	50.6	50.5	48.7	48.8	1.19	3.01	0.21	0.09
[310-330[	15.9	15.7	22.7	22.8	20.2	20.2	0.05	0.41	0.10	0.09
[330-350[	0.75	0.86	1.36	1.38	0.99	0.95	0.02	0.01	0.30	0.16

Table 4
Near the coast H_S frequency of occurrence (FO) at each directional bin (20°) for the historical (H) and future projected (F) ensembles, considering the 2041–2070 RCP4.5, 2071–2100 RCP4.5, 2041–2070 RCP8.5 and 2071–2100 RCP8.5 time-slices per bin of propagated-corrected coastal H_S and *MWD*.

Directions (°)	FO H Ofir (%)	FO F Ofir (%)	FO H Costa Nova (%)	FO F Costa Nova (%)	FO H Cova Gala (%)	FO F Cova Gala (%)	FO H Costa da Caparica (%)	FO F Costa da Caparica (%)	FO H Praia de Faro (%)	FO F Praia de Faro (%)
[350–10 [	0.08	0.09	0.06	0.05	0.01	0.04	0.01	0.01	0.45	0.42
		0.09		0.05		0.03		0.01		0.44
		0.09		0.04		0.03		0.01		0.44
		0.09		0.05		0.03		0.02		0.46
[10–30 [	0.09	0.10	0.10	0.09	0.01	0.01	0.01	0.01	0.94	1.02
		0.10		0.09		0.01		0.01		1.11
		0.10		0.09		0.01		0.01		1.15
		0.11		0.09		0.01		0.01		1.19
[30–50 [	0.14	0.18	0.11	0.09	0.01	0.01	0.01	0.01	0.55	0.62
		0.19		0.10		0.01		0.01		0.68
		0.19		0.10		0.01		0.01		0.70
		0.19		0.10		0.01		0.01		0.73
[50–70 [	0.01	0.01	–	0.01	0.01	0.01	0.02	0.01	0.07	0.09
		0.01		–		0.01		0.01		0.10
		–		–		0.01		0.01		0.10
		0.01		–		0.01		0.01		0.11
[70–90 [	–	–	–	–	–	0.01	–	–	–	0.01
		–		–		0.01		–		0.01
		–		–		0.01		–		–
		–		–		0.01		–		0.01
[90–110 [	–	–	–	–	–	–	–	–	–	–
		–		–		–		–		–
		–		–		–		–		0.01
		–		–		–		–		0.01
[110–130 [	–	–	–	–	–	–	–	–	0.01	0.02
		–		–		–		–		0.02
		–		–		–		–		0.02
		–		–		–		–		0.02
[130–150 [	0.01	0.01	–	–	–	–	0.30	0.32	4.21	4.43
		0.01		–		0.02		0.35		4.56
		0.01		–		0.02		0.36		4.61
		0.01		–		0.02		0.38		4.80
[150–170 [	–	0.01	–	–	–	–	0.15	0.18	15.7	15.0
		0.01		–		–		0.18		14.5
		–		–		–		0.19		14.2
		0.01		–		–		0.24		14.0
[170–190 [	–	–	–	–	–	–	0.14	0.17	5.04	4.66
		–		–		–		0.17		4.55
		–		–		–		0.18		4.49
		–		–		–		0.23		4.39
[190–210 [	0.09	0.09	–	–	–	0.01	0.62	0.76	0.49	0.46
		0.08		–		0.11		0.75		0.44
		0.08		–		0.08		0.80		0.44
		0.09		–		0.07		0.92		0.43
[210–230 [	1.30	1.35	0.41	0.40	0.26	0.43	9.70	9.15	2.24	2.15
		1.27		0.38		0.46		8.80		2.13
		1.31		0.35		0.45		8.63		2.13
		1.39		0.34		0.45		8.28		2.09
[230–250 [	2.17	2.07	1.21	1.14	1.06	1.16	41.8	40.6	32.1	31.3
		2.01		1.02		1.53		40.2		31.1
		1.97		1.04		1.38		40.1		31.1
		1.85		1.02		1.26		39.5		30.7
[250–270 [	6.80	6.09	3.10	2.66	2.31	2.79	35.9	36.2	32.0	33.1
		5.93		2.57		3.07		36.4		33.4
		5.73		2.42		2.80		36.4		33.5
		5.37		2.34		2.62		36.9		33.9
[270–290 [	32.0	31.6	20.4	19.4	26.4	27.2	7.99	8.77	5.96	6.36
		31.5		19.0		27.0		9.19		6.55
		31.4		18.8		26.9		9.30		6.62
		30.3		18.4		26.5		9.59		6.77
[290–310 [	40.7	41.0	50.5	51.1	48.8	47.3	3.01	3.35	0.09	0.09
		41.0		51.3		46.4		3.46		0.10
		41.2		51.6		46.6		3.50		0.10
		41.7		51.5		46.8		3.51		0.10
[310–330 [	15.7	16.4	22.8	23.5	20.2	20.1	0.41	0.44	0.09	0.09
		16.8		23.9		20.1		0.42		0.09
		16.9		24.0		20.3		0.44		0.09
		17.8		24.5		20.7		0.43		0.10
[330–350 [	0.86	0.94	1.38	1.53	0.95	0.98	0.01	0.02	0.16	0.19
		0.96		1.58		1.21		0.02		0.21
		0.96		1.58		1.38		0.02		0.22
		0.98		1.65		1.55		0.02		0.23

general behavior is similar to Ofir, with projections indicating enhanced frequency of lower H_S values (below 2 m), essentially incoming from northwards of 270° (W), compatible with the projected poleward displacement of the storm tracks, between 1.9% (2041–2070 under RCP4.5) and 3.4% (2071–2100 under RCP8.5). In terms of mean and 95% percentile H_S, values are generally projected to decrease northwards of 280° (WNW) and increase southwards. These projections are below 0.2 m, or ~10% (0.3 m, or ~7%) for the mean (95% percentile) H_S, except for the SSW-SW range (200°-230°), where differences between 0.1 and 0.3 m, or up to 50% (0.3–0.8 m, or up to 70%) are projected to occur. Note, however, that the SSW-SW *MWD* range corresponds to less than 1% of the total sample, and therefore integrated projections point to overall projected decreases, down to −3.79% (−4.20%) for the mean (95% percentile) H_S (Table SM11).

At Cova Gala (Table 4, and Fig. SM3 and Table SM8 in the SM), while the absolute mean and 95% percentile values are shown to be lower than for Ofir and Costa Nova, projections show similar patterns. Overall, H_S values below 1 m are projected to become more common, between 1.3% (2041–2070 under RCP4.5) and 2.5% (2071–2100 under RCP8.5). While higher wave heights are projected to become scarcer, the frequency of the most extreme H_S values is projected to remain almost unaltered (from 0.15% to 0.13–0.14% for H_S above 7 m). While a consistent increase in the frequency of waves incoming from S–W (190°-270°) is projected to occur for all wave heights, above 270° this behaviour is generally limited to H_S below 1 m. All scenarios project an increase of the extreme H_S southwards of 290°, generally within 0.1–0.3 m (5–20%). Furthermore, between WSW-WNW, increases between 0.2 and 0.4 m (7–12%) are also expected. Nevertheless, decreases are to be expected when considering the integrated mean and 95% percentile ensemble H_S, down to −4.42% and −3.73%, respectively (Table SM11).

At Costa da Caparica (Table 4, and Fig. SM4 and Table SM9 in the SM), across the most frequent *MWD* range (130°-330°), waves below 1 m are projected to become more frequent by 2.0% (4.2%) during 2041–2070 (2071–2100) under RCP4.5 (RCP8.5). For H_S values above 1 m, the opposite behaviour is projected. In contrast with Ofir, Costa Nova and Cova Gala, at Costa da Caparica the mean and 95% percentile H_S are projected to decrease throughout the entire directional range for all periods and scenarios, especially for *MWD* values below 210° (SSW). There, mean H_S differences between −0.1 m and −0.2 m (−10% to −20%) can be expected, and 95% percentile changes down to −0.75 m or −24% (−1.65 m or −54%) for the 2041–2070 RCP4.5 (2071–2100 RCP8.5) period are projected. It should be noted, however, that *MWD* s below 210° account for only 1–2% of the total samples. Hence, the overall integrated mean (95% percentile) H_S projections at Costa da Caparica do not exceed −5.65% (−5.13%) between future periods and scenarios (Table SM11).

For Praia de Faro (Table 4, and Fig. SM5 and Table SM10 in the SM), in the south-facing coast of Portugal, similarly to the remaining key-locations, waves below (above) 0.5 m H_S are projected to become more common (scarce) in between 2.2% and 3.9%, for the 2041–2070 RCP4.5 and 2071–2100 RCP8.5 periods, respectively. Projected changes in the mean and 95% percentile H_S follow a similar behaviour at Praia de Faro, showing consistent decreases throughout most of the incoming directional range (except between 300° and 310°; NW). Thus, the integrated future H_S projections for the ensemble mean and 95% percentile attain differences as low as −7.04% and −7.10%, respectively (Table SM11).

Finally, the associated SLR projections were extracted from the 21-member ensemble for each future time-slice and scenario, at the closest grid-point to each key-location. The obtained SLR values are summarized in Table SM12 in the SM.

3.3. ShorelineS performance evaluation (2008–2018)

The ability of the ShorelineS model to represent the complex processes driving shoreline evolution is evaluated by forcing it with hydrodynamic conditions from the nearshore bias corrected ERA5 (H_S, T_m and *MWD*), from 2008 to 2018, and shown in Fig. 4. This time window corresponds to two moments where aerophotogrammetric data and field data is available and can be used to produce initial and final shoreline positions, based on real observations. Note, however, that this free shoreline evolution does not account for local human intervention processes, although considering pre-existent structures, like groins, SLR (estimated at approximately 3.6 cm in the Cascais tide gauge) or tides. Therefore, differences are expected to arise, especially along artificialized coastal segments.

At Ofir (Fig. 4a), the evaluation process revealed very reasonable results in all coastal segments (between each set of groins). The effective littoral drift at Ofir is significantly lower than the potential drift, and therefore a manual calibration based on the coastline retreat rates described by Lira et al. (2016) was performed to promote a better agreement with observations. Overall, an average longitudinal bias (mean absolute error; MAE) of −0.90 m (13.1 m) was obtained.

At Costa Nova, the evaluation of the ShorelineS model produced good results between 2008 and 2018 (Fig. 4b), especially south of the first groin, where human intervention is less frequent. Northwards of this structure, performance is slightly reduced, due to the numerous beach nourishment activities conducted there during the analysed time-window (Pinto et al., 2020). Nevertheless, the overall model performance is considered reasonable for the adopted parameterization, with a mean bias (MAE) of 3.50 m (22.9 m) for the area.

Along the Cova Gala stretch (Fig. 4c), ShorelineS also represents the observed shoreline evolution reasonably, in both the northerly (open sandy beaches) and southerly (enclosed beaches limited by groins and adherent structures) portions of the coastline. The performance is, nevertheless, lower in the top North of the domain. This is possibly due to the beach nourishment interventions conducted in that location during the analysed time-window (Pinto et al., 2020), or other local effects, such as wave diffraction from Cape Mondego, potentially driving sediment northwards in this area. Overall, an overestimation of the retreat by 11.8 m on average (MAE of 12.4 m) is observed.

For Costa da Caparica (Fig. 4d), the ShorelineS model is able to reasonably depict the historical evolution of the shoreline, with very small differences overall, especially South of São João da Caparica beach, where the observed 2018 shorelines are generally very close to the simulated ones, after 10 years (differences below 10 m). In the northern portion of the area, however, differences attain larger values, possibly due to local higher nartural variability range of the system related the effects of the Tejo river's sedimentary delta, inducing very localized changes in wave direction, favouring periods of sedimentary accretion. There, the results show exacerbated shoreline retrats in comparison with the 2018 observation, of up to 90 m. Nevertheless, it should be noted that artificial beach nourishments took place in Costa da Caparica in 2008, 2009 and 2014 (Pinto et al., 2020). Overall, the mean areawide bias (MAE) is set at 9.90 m (31.9 m).

Finally, at Praia de Faro (Fig. 4e), the behavior of the shoreline can be considered relatively homogeneous during the evaluation period, due to its naturally linear configuration, and the absence of hard human interventions. For these reasons, Praia de Faro reveals the best overall ShorelineS performance, with differences consistently below 20 m when compared with the actual observed shoreline by 2018. The mean shoreline bias and the MAE are set at −3.90 m and 5.70 m, respectively, indicating slightly reduced simulated retreat.

All considered, the ShorelineS performance is good for the adopted parameterizations, providing the necessary confidence in the model to project the natural evolution of the shoreline along the five key-locations throughout the 21st century.

3.4. Future projected shorelines towards the end of the 21st century

Table 5 summarizes the ensemble mean potential longshore sediment transport (LST) projections for both the RCP4.5 and RCP8.5

Fig. 4. (a) Ofir, (b) Costa Nova, (c) Cova Gala, (d) Costa da Caparica and (e) Praia de Faro observed shoreline (2008 – blue dashed line, and 2018 – black dashed line) *versus* modelled shoreline in 2018 from 2008 initial conditions, forced by the propagated-corrected-propagated ERA5 reanalysis (red line). Relevant locations as well as the areawide MAEs are overlayed.

scenarios across each of the key-locations, during the 21st century (2011–2100), divided into three time-slices (2011–2040, 2041–2070 and 2071–2100), showing also the mean yearly trend throughout the entire period. Values are positive for southward transport, and negative for northward.

3.4.1. *Ofir*

The projected LST rates throughout the 21st century, at the Ofir key-location, for the 6-member ensemble (mean and uncertainty range) under the RCP4.5 and RCP8.5 scenarios, are shown in Fig. 5. Such analysis provides an indication of the sediment amount that is being carried off the area yearly, with direct implications for long-term beach nourishment planning. The projected rates are positive (*i.e.*, southwards net transport), with an ensemble mean value of 1.251×10^6 m^3/year (1.247×10^6 m^3/year) for the RCP4.5 (RCP8.5) scenario during 2011–2040 (Table 5). For the medium- and long-term, the ensemble mean LST rates are projected to consistently decrease (agreement of at least 5 in 6 members) for both scenarios, towards 1.166×10^6 m^3/year (1.190×10^6 m^3/year) during 2041–2070 and 1.127×10^6 m^3/year (1.205×10^6 m^3/year) during 2071–2100. Between scenarios, the larger mean projected LST rates for the RCP8.5 are compatible with an enhancement of the northward component in the local wave climate, associated to most sea state conditions (Table 4, Fig. SM1 and Table SM6 in the SM). From 2011 to 2100, a mean trend of -2000 m^3/year^2 (-700 m^3/year^2) is identified, for the RCP4.5 (RCP8.5) scenario (Table 5).

The projected Ofir shorelines forced exclusively by wave climate projections are depicted in Fig. SM6 of the SM. Different behaviors are projected due to wave action. In the northern sector (North of the first

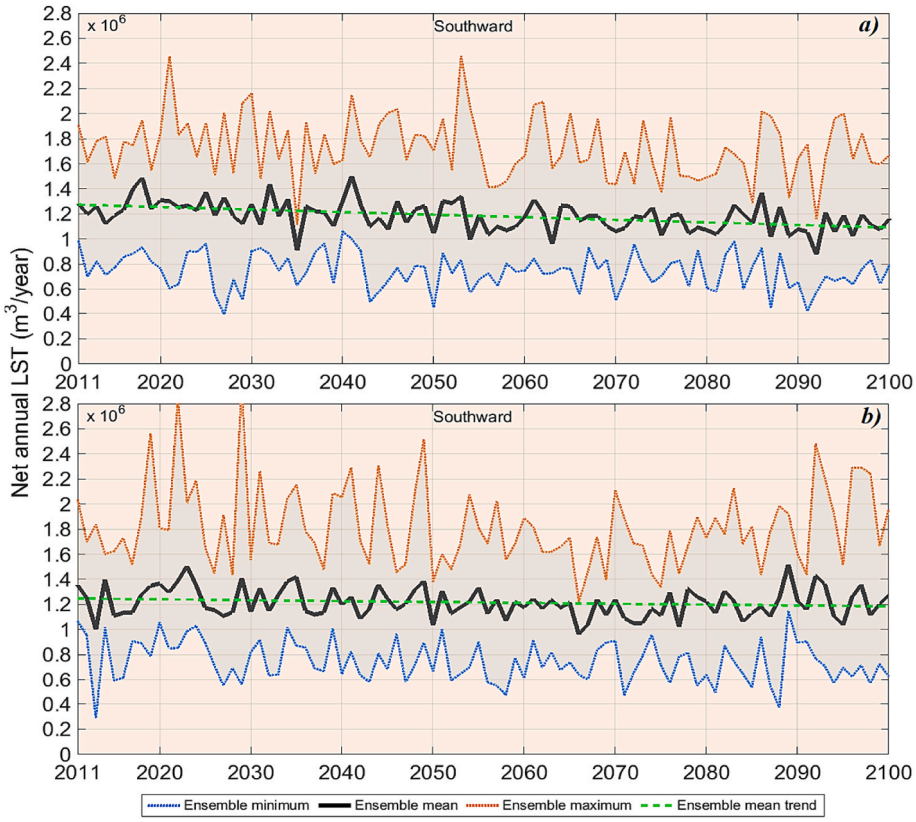

Figs. 5. 21st century projected LST yearly rates (m^3/year) at the Ofir key-location for the (a) RCP4.5 and (b) RCP8.5 scenarios.

Table 5
Ensemble mean LST projections (10^6 m^3/year) at each of the key-locations for the RCP4.5 and RCP8.5 scenarios throughout the 21st century, and ensemble mean yearly trend during 2011–2100 (10^6 m^3/$year^2$).

LST ensemble mean (10^6 m^3/year) and trend (10^6 m^3/$year^2$)				
RCP4.5				
	2011–2040	2041–2070	2071–2100	Trend
Ofir	1.251	1.166	1.127	−0.0020
Costa Nova	0.820	0.783	0.805	−0.0003
Cova Gala	0.960	0.880	0.858	−0.0017
Costa da Caparica	−0.527	−0.489	−0.435	0.0014
Praia de Faro	−0.083	−0.078	−0.066	0.0030
RCP8.5				
	2011–2040	2041–2070	2071–2100	Trend
Ofir	1.247	1.190	1.205	−0.0007
Costa Nova	0.861	0.855	0.803	−0.0008
Cova Gala	0.838	0.805	0.748	−0.0015
Costa da Caparica	−0.511	−0.438	−0.378	0.0024
Praia de Faro	−0.079	−0.062	−0.053	0.0050

groin), a slight northwards rotation is visible, with areas of consistent accretion (retreat) between ensemble members, compatible with *MWD* projections. In the central sector (Praia de Ofir), rotation is not so evident, with enhanced projected erosion south of the first groin. In the southern sector (Praia da Bonança and Praia de Fao), shoreline retreat is also projected to be dominant, despite small areas of accretion.

The final projected shorelines, considering both the effects of the wave climate (ensemble mean shoreline) and SLR under the RCP4.5 and RCP8.5 scenarios are depicted in Fig. 6. SLR unequivocally suppresses all "virtual accretion" zones resulting from wave action alone (especially north of the first groin), leading to robust projected shoreline retreat along most of the domain extension (the areas showing no retreat represent no accommodation space), assuming no human intervention or beach nourishments during the 21st century.

Under the RCP4.5 (Fig. 6a), by 2070 (2100), retreat from the 2018 reference line of up to 60 m (100 m) at Praia de Ofir, south of the first groin, 80 m (100 m) at Praia da Bonança, south of the second groin, and 70 m (70 m) at Praia de Fao, north of the third groin, is projected. For the RCP8.5 (Fig. 6b), retreat of up to 80 m (120 m) at Praia de Ofir in 2070 (2100) and no less than 30 m (60 m) north of the second groin is projected to occur. At Praia da Bonança, 90 m (120 m) retreat can be expected, whereas at Praia de Fao values are slightly lower, but still ranging between 50 m and 80 m. Particularly at Praia de Ofir and Praia da Bonança, under the RCP8.5, the shoreline is likely to retreat towards urban areas, even considering the moderate RCP4.5 scenario.

3.4.2. *Costa Nova*

The projected LST rates at Costa Nova towards 2100 are shown in Fig. 7. These projections reveal a constant southwards net transport, with an ensemble mean of 0.820 × 10^6 m^3/year (0.861 × 10^6 m^3/year) for the RCP4.5 (RCP8.5) during 2011–2040. Ensemble mean LST rates are projected to consistently decrease (agreement of at least 3 in 6 members) for both scenarios, towards 0.783 × 10^6 m^3/year (0.855 × 10^6 m^3/year) during 2041–2070 and 0.805 × 10^6 m^3/year (0.803 × 10^6 m^3/year) during 2071–2100 (Table 5). Similarly to Ofir (Fig. 5), higher mean projected LST rates for the RCP8.5 are compatible with an enhancement of the northward component in the local wave climate, associated to most sea state conditions (Table 4, Fig. SM2 and Table SM7 in the SM). From 2011 to 2100, a mean trend of −300 m^3/$year^2$ (−800 m^3/$year^2$) is identified, for the RCP4.5 (RCP8.5) scenario (Table 5).

The projected shorelines at Costa Nova forced exclusively by wave climate projections are shown in Fig. SM7 in the SM. Overall, the shoreline behavior is marked by a slight northwards rotation, compatible with the projected change in *MWD*. The impact of the groins is clearly visible, with areas of consistent accretion (retreat) North (South)

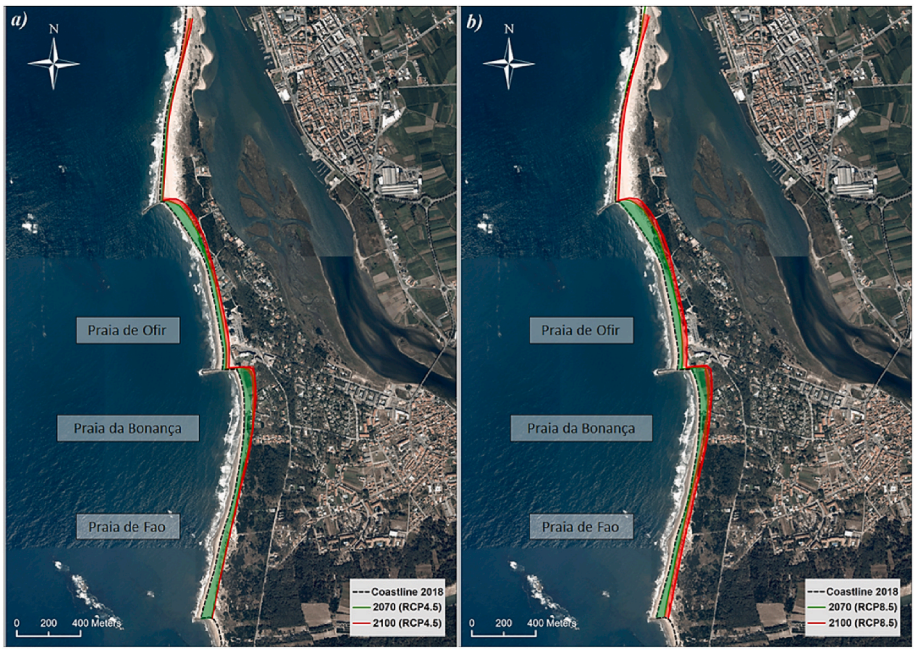

Fig. 6. Projected mean shorelines at Ofir forced by the propagated-corrected ensemble of wave climate projections by (green) 2070 and (red) 2100 (snapshots) under the (a) RCP4.5 and (b) RCP8.5 scenarios, including the effects of SLR (mean projection). The black dashed line represents the reference shoreline (2018). Relevant locations are overlayed.

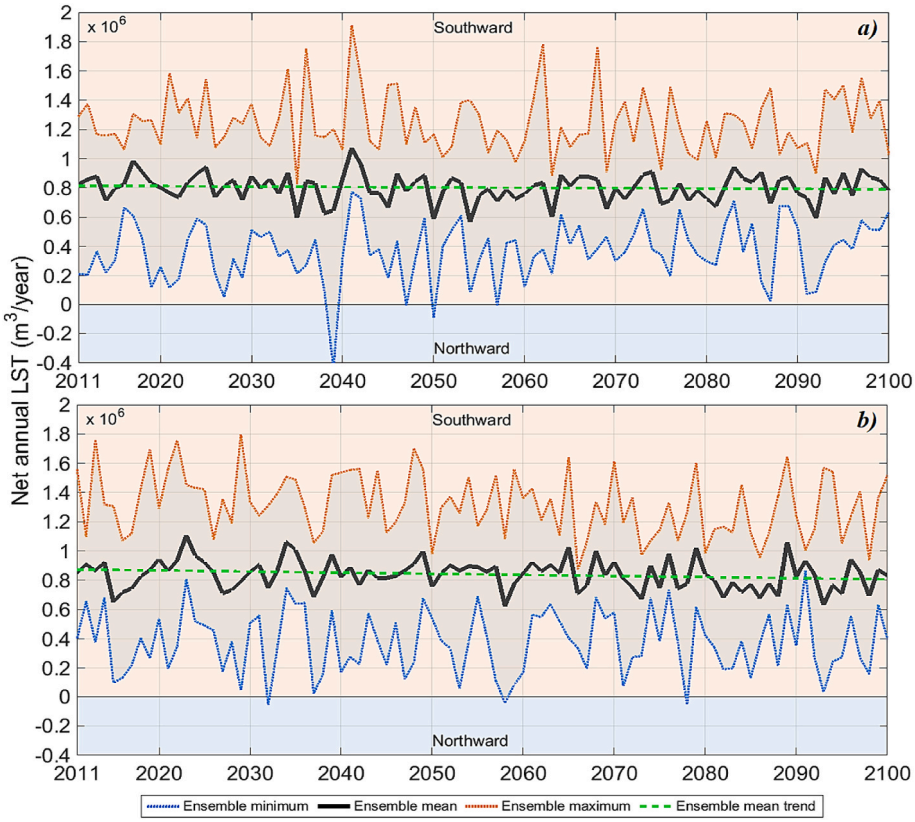

Fig. 7. Same as in Fig. 5, but for the Costa Nova key-location.

of each structure. This behavior is consistent for all ensemble members.

Fig. 8 shows the same as Fig. 6, but for Costa Nova. Considering SLR, consistent projected shoreline retreat is visible along the entire extension of the Costa Nova study area domain. Under the RCP4.5 (Fig. 8a), by 2070 (2100), values amount to 170 m (200 m) at Praia Velha, 80 m (105 m) south of the first groin (Praia da Costa Nova - North), 60 m (90 m) south of the second groin (Praia da Costa Nova - South) and 80 m (105 m) south of the third groin (Praia Nova), from the 2018 reference line. Under RCP8.5 (Fig. 8b), by 2100, maximum shoreline retreat of 210 m, 110 m, 70 m and 110 m is expected at Praia Velha and south of

Fig. 8. Same as in Fig. 6, but for the Costa Nova key-location.

the first, second and third groins (North to South), respectively. Such results reveal projected shorelines within urban areas at several locations along Costa Nova.

3.4.3. Cova Gala

At Cova Gala, the projected LST rates follow a similar trend to the ones of Costa Nova, showing a slight but consistent projected decrease (agreement of at least 4 in 6 members) towards 2100 (Fig. 9), from a mean ensemble value of 0.960 × 10^6 m^3/year (0.838 × 10^6 m^3/year) during 2011–2040, to 0.880 × 10^6 m^3/year (0.805 × 10^6 m^3/year) during 2041–2070 and 0.858 × 10^6 m^3/year (0.748 × 10^6 m^3/year) during 2071–2100 under the RCP4.5 (RCP8.5) scenario (Table 5). The overall trend is slightly more expressive for the RCP4.5 scenario, at −1700 m^3/$year^2$, in comparison with −1500 m^3/$year^2$ found for the

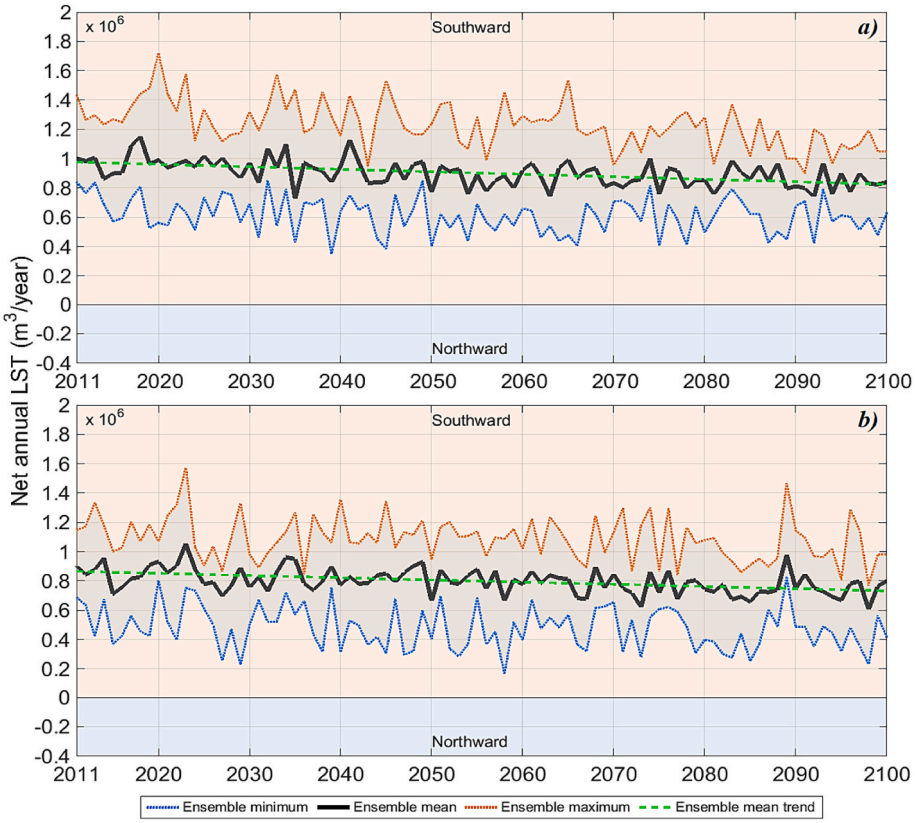

Fig. 9. Same as in Fig. 5, but for the Cova Gala key-location.

RCP8.5. Nevertheless, a continued erosion process at Cova Gala is expected.

The impact of future projected wave action at Cova Gala's shorelines is shown in Fig. SM8 in the SM. Similarly to Costa Nova, a slight northwards shoreline rotation is visible, especially in the northern half of the area, consistent between all ensemble members. The five groins positioned directly off Cova Gala offer additional protection against extreme coastal erosion and rotation associated to future projected wave climate. In terms of shoreline retreat, the most affected area is located at the top of the domain, at Praia do Cabedelo. Not surprisingly, in the areas where a fixed barrier already exists (at the beaches adjacent to the village), shoreline is not projected to change significantly.

Fig. 10 is similar to Fig. 6, but for Cova Gala. Closely to Costa Nova, the "virtual" sediment accretion is no longer projected North of the first groin with the inclusion of SLR. Under the RCP4.5 scenario (Fig. 10a), retreat values become higher, up to 90 m (140 m) at Praia do Cabedelo, 60 m (80 m) at Praia de Cova Gala Norte (directly affecting urbanized area near "Hospital Distrital da Figueira da Foz"), and 80 m (110 m) in the northern portion of Praia de Cova Gala Sul (also directly affecting urbanized area), from the 2018 reference values, by 2070 (2100). Considering the RCP8.5 (Fig. 10b), shoreline retreat up to 110 m (150 m) at Praia do Cabedelo, 70 m (90 m) at Praia de Cova Gala Norte and 90 m (120 m) at Praia de Cova Gala Sul is expected. Such projected evolution represents a major risk for Cova Gala, in the case of no human intervention, with the shoreline expected to lay inside urban areas in several locations along the domain.

3.4.4. Costa da caparica

Fig. 11 is similar to Fig. 5, but for the Costa da Caparica key-location. Throughout the 21st century, LST rates are projected to be negative (representing an overall northwards sediment transport), showing, nevertheless, a slight but consistent projected decrease (agreement of at least 4 in 6 members) in magnitude, from a mean ensemble value of -0.527×10^6 m^3/year (-0.511×10^6 m^3/year) in the 2011–2040 period, to -0.489×10^6 m^3/year (-0.438×10^6 m^3/year) during 2041–2070 and -0.435×10^6 m^3/year (-0.378×10^6 m^3/year) during 2071–2100 (Table 5). This tendency is especially noticeable for the RCP8.5 scenario (Fig. 11b), at 2400 m^3/year^2, in comparison with 1400 m^3/year^2 found for the RCP4.5 (Fig. 11a).

The projected Costa da Caparica shorelines resulting from projected wave action are shown in Fig. SM9 in the SM. In the central and southern portions of the area, shorelines are projected to remain stable due to the existence of a long seawall extending from Praia de São João da Caparica onto Nova Praia, covering approximately 3 km. In the northern portion, however, from Praia da Cova do Vapor to Praia de São João da Caparica, extensive consistent retreat is projected to occur from wave action alone, ranging between 160 m and 220 m between ensemble members, for all future periods and scenarios. Such behavior, despite possibly amplified by the results of Fig. 3, is compatible with the *MWD* projections for this area, indicating a slight northwards rotation (Table 4, Fig. SM4 and Table SM9), allowing extensive erosion on the northernmost stretch of Praia de São João da Caparica, which is oriented to the SW. In fact, it was shown that while the SW (210-230°) component of the wave climate at this study location is projected to decrease, from 9.70% during the historical period, towards 9.16%, 8.80%, 8.63% and 8.28%, during 2041–2070 and 2071–2100, under RCP4.5 and RCP8.5, respectively, the W (250-270°) component is projected to increase, from 35.87% (historical), towards 36.15%, 36.45%, 36.43% and 36.84%, respectively (Table 4). These changes, along with the ones for the remaining sectors, might exacerbate the erosive processes in southward-facing beaches, such as in the northern portion of Praia de São João da Caparica.

The compound shoreline projections from wave climate and SLR are shown in Fig. 12. Overall, shoreline retreat can be observed throughout Costa da Caparica for all future periods and scenarios. Between them, differences are generally small, due to the long seawalls protecting the urban areas facing the ocean, with almost no accommodation space left. In Fig. 12, retreat of up to 60 m by 2070 (80 m by 2100) between Nova Praia and Praia da Saúde, and 100 m (100 m) in Praia do Dragão Vermelho and Praia Nova (central and southern urban area of Costa da Caparica) is visible, for both scenarios. At Praia de São João da Caparica, near Cova do Vapor, retreat of up to 280 m (290 m) is projected under the RCP4.5, reaching 300 m under the RCP8.5 by 2100. Such projections contrast with the expected accretion in the southern portion of this beach, within 40–60 m between scenarios. Note, however, that these projected accretions lie close to the error margin found for this section in Fig. 3. Particularly for the RCP8.5 (Fig. 12b), at Praia da Cova do Vapor (top North of the domain), the shoreline is projected to remain stable under this scenario, whereas under the RCP4.5 (RCP8.5), retreat of up to

Fig. 10. Same as in Fig. 6, but for the Cova Gala key-location.

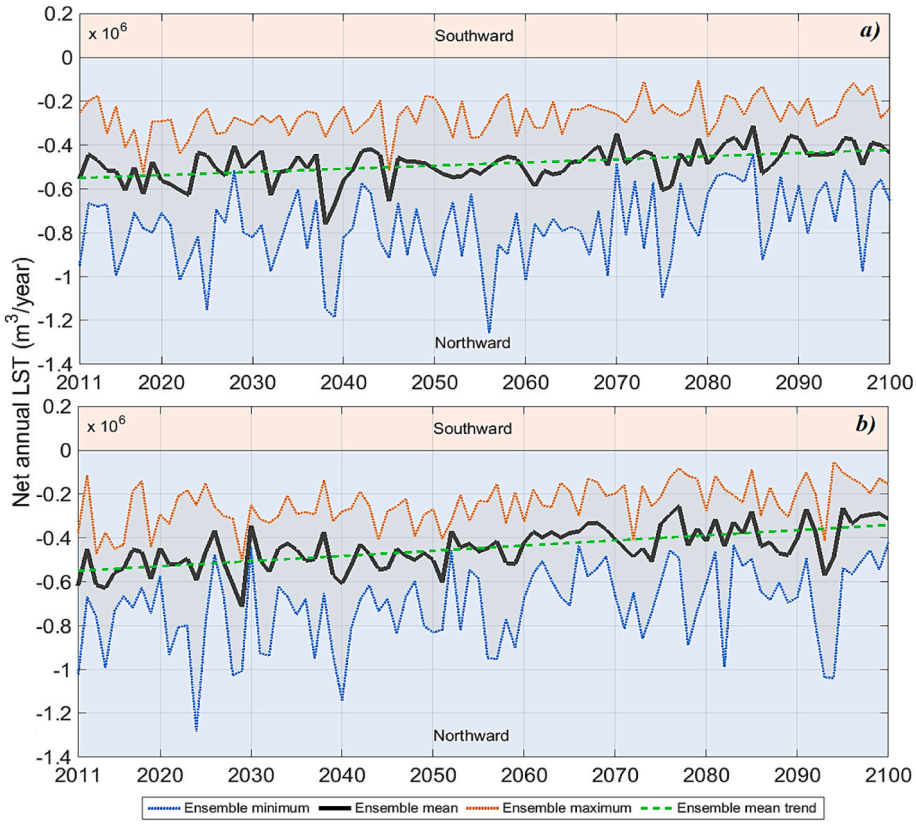

Fig. 11. Same as in Fig. 5, but for the Costa da Caparica key-location.

Fig. 12. Same as in Fig. 6, but for the Costa da Caparica key-location.

170 m (190 m) is expected to occur, demonstrating increased sensitivity even to slight changes in the *MWD*. It should, nevertheless, be recalled that the projections for the northern portion of the domain should be interpreted with caution due to the local model limitations found in the evaluation process.

3.4.5. *Praia de faro*

The projected LST rates at Praia de Faro towards 2100 are shown in Fig. 13. These assume mostly negative values (*i.e.*, northwards net transport, in this case, with a reduced northward component, in a slow northwesterly transport), with an ensemble mean of -0.083×10^6 m^3/

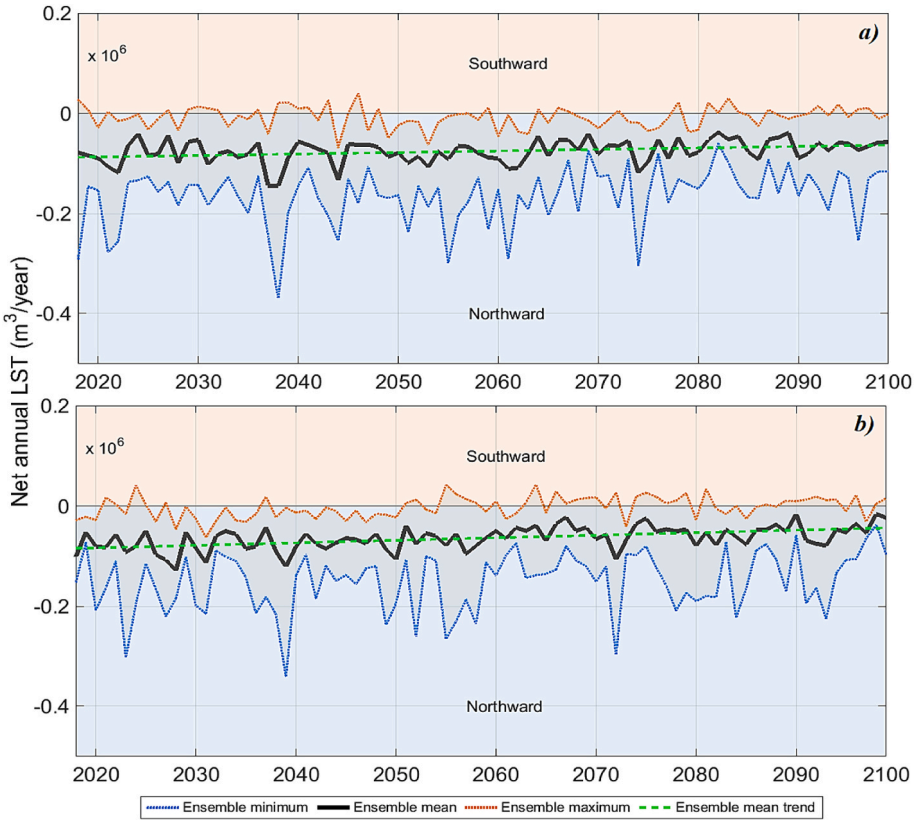

Fig. 13. Same as in Fig. 5, but for the Praia de Faro key-location.

year (-0.079×10^6 m^3/year) for the RCP4.5 (RCP8.5) during 2011–2040. Overall, ensemble mean LST rates are still projected to consistently decrease (agreement of at least 3 in 6 members) for both scenarios, towards -0.078×10^6 m^3/year (-0.062×10^6 m^3/year) during 2041–2070 and -0.066×10^6 m^3/year (-0.053×10^6 m^3/year) during 2071–2100. Throughout the 21st century, the lower mean projected LST rates for the RCP8.5 are compatible with the local projected decrease in wave energy. From 2011 to 2100, a mean trend of 3000 m^3/year^2 (5000 m^3/year^2) is identified, for the RCP4.5 (RCP8.5) scenario (Table 5).

The shorelines at the Praia de Faro key-location, composed of long sandy beaches, are projected to change almost uniformly with wave action towards 2100 (Fig. SM10 in the SM). The expected retreat is greater where the accommodation space allows, *i.e.*, away from the most densely populated area. The erosion related to wave action alone is projected to be kept below 30 m by 2070 under RCP4.5, and range between 20 m and 60 m by 2100, under RCP8.5. Between ensemble members, uncertainty is low (generally below 20 m, and the lowest between the five key-locations), given the geomorphological homogeneity of the area (without natural adherent structures of hard-human interventions) and the dynamics of the regional wave climate, with less extreme events and less directional variability than in the other locations.

Fig. 14 is similar to Fig. 6, but for Praia de Faro. The long low sandy beaches without artificial structures that characterize this key-location allow a consistent retreat to be expected throughout the entire area, depending (almost exclusively) on the SLR values. Overall, shoreline retreat is visible at Praia de Faro, for all future periods and scenarios. Differences are related to the magnitude of the SLR, with maximum values ranging between 20 m and 35 m by 2070 under RCP4.5, and 50 m and 80 m for 2100 under RCP8.5.

4. Discussion and conclusions

This study provided the first consistent, ensemble-based assessment of coastal erosion and shoreline evolution projections for Portugal, from a large set of CMIP5 data. A 6-member ensemble of wave climate projections, propagated nearshore to account for the effects of local bathymetry and bias corrected using an innovative and streamlined methodology based on a synergic combination of reanalysis and observational data, was used. Additionally, a 21-member ensemble of SLR projections was utilized to drive the ShorelineS model and produce high-resolution shoreline projections along five Portuguese highly vulnerable key-locations, towards the end of the 21st century. The coastal environments considered are characterized by sandy coastlines, often with anthropized segments marked by adherent structures and groins.

Regarding wave climate, nearshore H_S and *MWD* projections, as represented by the coastal propagated-corrected ensemble at each of the five key-locations, were summarized in Table 4. Overall, low northerly (high westerly) waves are projected to become more frequent (scarcer) in the future. Such behavior is consistent with the enhanced projected decreases in the mean H_S values along the eastern North Atlantic described by Lemos et al., 2021b and others (*e.g.* Dobrynin et al., 2015; Perez et al., 2015; Gallagher et al., 2016; Aarnes et al., 2017; Camus et al., 2017; Casas-Prat et al., 2018; Webb et al., 2018; Morim et al., 2018, 2019; Lemos et al., 2019, 2020a). At Ofir and Costa Nova, the frequency increases of northerly waves ranged from 1.08% to 4.22% at Ofir, and 1.45%–2.97% at Costa Nova, considering the 2041–2070 RCP4.5 and 2071–2100 RCP8.5 future projected periods (Table 4). At Cova Gala, projections also showed an increase in frequency for *MWD* s within 190°-290° (SSW-WNW, especially for the RCP4.5 2071–2100 future period, at 2.15%), in addition to the slight increase for the 310°-350° (NW–N) interval. In Costa da Caparica, directional frequency projected increases also revealed a bimodal behavior across 130°-210° (SE-SW) and northwards of 250° (WSW). The projected frequency

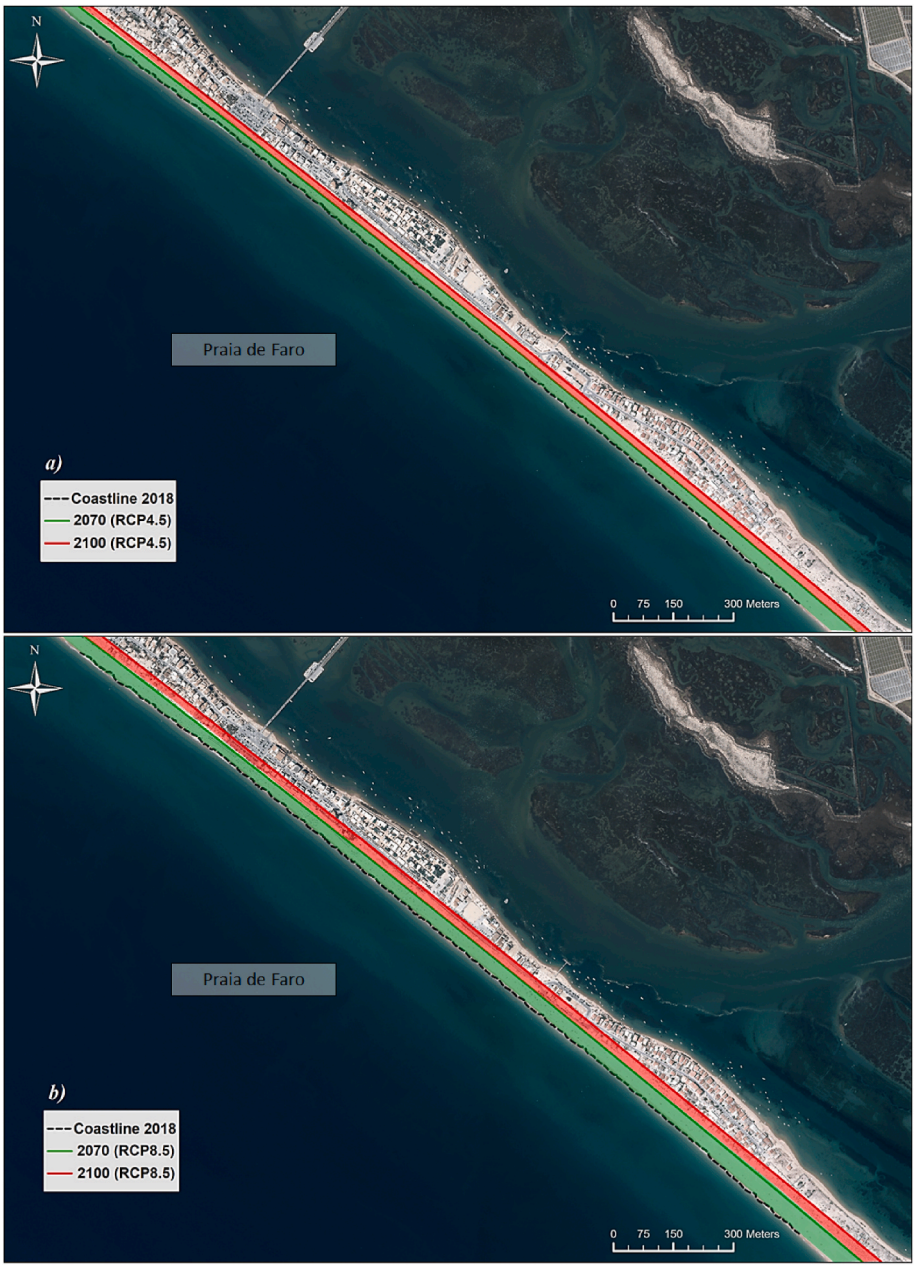

Fig. 14. Same as in Fig. 6, but for the Praia de Faro key-location.

decreases between 210° and 250° ranged from −1.75% (2041–2070 RCP4.5) to −3.72% (2071–2100 RCP8.5). Finally, at Praia de Faro, a decrease in the frequency of occurrence of *MWD* s southwards of 250° (WSW) has been found, except for the 130°-150° range (SE-SSE). Northwards of 250°, projected increases between 1.53% (2041–2070 RCP4.5) and 2.80% (2071–2100 RCP8.5) were shown to occur. It should be noted, nevertheless, that across Costa da Caparica and Praia de Faro, the ensemble slightly underestimated the southwesterly components while overestimating the westerly ones, even after the propagation-correction procedure (Table 3).

The ability of the ShorelineS model to accurately depict shoreline evolution was assessed by reproducing the observed shoreline by the year 2018 from 2008 initial conditions (two moments where observations were available) using the propagated-corrected-propagated ERA5 reanalysis data. Overall, the performance assessment revealed a good agreement with observations, with mean biases and MAEs ranging between −3.90 m and 11.8 m, and 5.70 and 31.9 m, respectively, and a generally better (poorer) representation at Praia de Faro (Costa da Caparica).

Future ensemble mean shoreline projections were showed in Figs. 6, 8, 10, 12 and 14 for the five selected key-locations, considering the joint effects of SLR and wave action towards 2100. Future projected shorelines considering wave action alone from the 6-member ensemble were also shown in Figs. SM6 to SM10 in the SM. Such an ensemble approach provided a useful tool to better quantify the uncertainty associated with the multi-model dynamic forcing and evaluate the robustness of the final mean shorelines.

There is an increasing need for physics-based shoreline evolution models able to quantify the contribution of waves to local changes in morphology in the context of continuously changing sea levels (Montaño et al., 2020; D'Anna et al., 2021). Here, the Bruun's rule was applied *a posteriori* to the wave-driven shoreline projections from ShorelineS, in the absence of a different validated formulation for SLR-induced shoreline retreat. According to D'Anna et al. (2022), when

the Bruun rule's assumptions are satisfied, results from wave-driven models (such as ShorelineS) combined separately with the Bruun rule (without continuous feedback) are able to implicitly represent the primary processes driving long-term sea-level-induced shoreline retreat. Despite its limitations, Bruun's rule has seen widespread usage in scientific literature over the last decades and has been successfully validated under laboratory conditions (Atkinson et al., 2018). Furthermore, the five key-locations considered here represent mainly beach-dune environments with considerable accommodation space, in line with most of Bruun's rule assumptions. Exceptions were shown to occur along short, urbanized stretches, where seawalls were considered fixed structures and further shoreline retreat was manually prevented.

Two main conclusions can be drawn from our results: 1) future nearshore wave action, projected to become more northerly and less energetic, is projected to lead to northward beach rotations especially along the northern and central Portuguese coastal stretches (Ofir, Costa Nova and Cova Gala, in Figs. SM8 to SM10), promoting areas of "virtual accretion"; 2) the projected SLR effectively suppresses most of these accretion zones, leading to consistent projected shoreline retreat throughout all key-locations. These results are in agreement with several studies indicating that while wave action is projected to dominate morphological response until the mid-21st century, SLR is expected to become the main driver of shoreline evolution beyond that time-frame (Howard et al., 2019; D'Anna et al., 2021, 2022; Hunt et al., 2023 and Table SM13). Final projected shoreline retreats were shown to locally reach 100 m (120 m) by 2100 under RCP4.5 (RCP8.5) at Ofir (Figs. 6), 200 m (210 m) at Costa Nova (Figs. 8), 140 m (150 m) at Cova Gala (Figs. 10), 290 m (300 m) along Costa da Caparica (Figs. 12) and 65 m (80 m) in Praia de Faro (Fig. 14).

Considering the mean behavior across the entire domain of each key-location, the average areawide projected shoreline retreat and ensemble inter-member uncertainties are depicted in Table 6, together with the overall projected lost area between reference (2018) and future mean projected shorelines. While all mean retreats can be considered robust (exceeding the ensemble inter-member uncertainty range), Costa Nova shows the greatest uncertainty range between ensemble members. For the 2041–2070 future period, mean areawide retreats range between 26.6 m and 60.7 m (30.1 m and 53.7 m) under RCP4.5 (RCP8.5), whereas for 2071–2100 these range between 44.4 m and 84.2 m (43.7 m and 81.6 m). These are often greater for the RCP4.5 scenario, mainly due to increased beach rotation projected under RCP8.5, with the addition of "virtual accretion" areas, immediately north of groins or other fixed structures that, although offset by SLR, contribute to reduced mean shoreline retreat overall. In addition to the projected changes in the nearshore waves' *MWD*, enhanced projected decreases in mean wave energy under RCP8.5 (Table 4, Figs. SM1 to SM5 and Table SM11) were shown to result in lower LST rates than under RCP4.5 at Cova Gala, Costa da Caparica and Praia de Faro (Table 5 and Figs. 7, 9 and 11). Such results indicate that a future climate trajectory under higher-emission scenarios could potentially reduce the local need for beach nourishment interventions, especially along the central and southern Portuguese coastal areas. Absolute LST rates are, nevertheless, projected decrease along all key-locations, independently of the scenario, between −0.04% and −6.33%.

Finally, the projected lost areas between reference (2018) and future mean shorelines range between 0.088 km^2 and 0.184 km^2 (0.118 km^2 and 0.197 km^2) by 2100, under RCP4.5 (RCP8.5), the smallest (greatest) losses expected to take place at Faro and Cova Gala (Costa Nova). Throughout all key-locations (approximately 14 km of coastline), the cumulative amount of projected lost area from 2018 to 2100 is 0.786 km^2, relevant when compared to the historical nationwide area lost to the sea between 1958 and 2021, which amounted to 13.5 km^2 for over 980 km of coastline.

The results from this study should be interpreted as a baseline projection for the Portuguese sandy coastlines, maintaining the current coastal defense structures with no additional coastal protection and risk-reduction measures implemented (inaction scenario). Note that domains covered by this study comprise only a portion of the Portuguese sandy coastlines (3.38%), which, according to Pinto et al. (2020), span for about 414 km. Although similar behavior can be expected from the remaining Portuguese sandy coastlines, specific analyzes are required for different coastal environments (*e.g.*, rocky cliffs and pocket beaches, soft cliffs and low rocky environments, occurring on 58% of the coastline; Pinto et al., 2020).

Future Portuguese adaptation and mitigation measures should rely on "worst-case scenario" information to base their strategies and expect continuous changes well beyond the end of the 21st century (Lyon et al., 2022), anticipating additional levels of protection to be implemented in the future. Naturally, the effects of climate change along the coasts are not limited to shoreline retreat, and an increased risk of extreme coastal flooding must also be considered.

The combination of coastal retreat with high-frequency flooding could result in loss of coastal ecosystems and fertile soil for agriculture, given the potential landward intrusion of saltwater, besides the imminent risks for human life. From an economic perspective, the erosion of sandy coastal segments presents a serious problem, as areas relevant for tourism diminish in size or are lost over time. Furthermore, accommodating adherent structures or urban infrastructure to ensure resiliency against changes in the water levels requires vast economic resources, which are generally not available. Our results, based on multi-model, multi-process and multi-scenario approaches, play a crucial role in the design of a complete climate change impact assessment for the Portuguese coastal areas, vital for adequate coastal managements and adaptation planning.

Table 6
Mean projected shoreline retreat (m) and mean ensemble inter-member uncertainty (m), and lost area from reference (2018) shoreline (km^2) along each key-location, considering the 6-member ensemble of shoreline projections driven by projected wave action and SLR. Projected values are extracted at the last year of each time-slice (2070 and 2100). Robust projected shoreline retreat (greater than the inter-member uncertainty) is underlined.

Mean shoreline retreat (mean ensemble uncertainty; m)				
	2070 (RCP4.5)	2070 (RCP8.5)	2100 (RCP4.5)	2100 (RCP8.5)
Ofir	39.5 (13.6)	30.7 (15.9)	51.9 (22.0)	56.2 (19.2)
Costa Nova	60.7 (31.8)	50.2 (37.5)	84.2 (32.2)	81.6 (44.5)
Cova Gala	48.4 (23.7)	53.7 (21.5)	67.8 (17.5)	77.0 (19.9)
Costa da Caparica	42.9 (25.7)	30.1 (27.5)	54.9 (19.6)	43.7 (25.8)
Praia de Faro	26.6 (13.3)	35.7 (12.7)	44.4 (13.8)	62.7 (11.1)
Lost area from reference (2018) shoreline (km^2)				
	2070 (RCP4.5)	2070 (RCP8.5)	2100 (RCP4.5)	2100 (RCP8.5)
Ofir	0.092	0.089	0.157	0.188
Costa Nova	0.105	0.104	0.184	0.197
Cova Gala	0.071	0.081	0.103	0.118
Costa da Caparica	0.142	0.120	0.175	0.164
Praia de Faro	0.052	0.071	0.088	0.119
Total	0.462	0.465	0.597	0.786

CRediT authorship contribution statement

Gil Lemos: Writing – review & editing, Writing – original draft, Methodology, Investigation, Formal analysis. **Ivana Bosnic:** Writing – review & editing, Software, Resources, Formal analysis. **Carlos Antunes:** Writing – review & editing, Resources, Funding acquisition, Conceptualization. **Michalis Vousdoukas:** Writing – review & editing, Data curation. **Lorenzo Mentaschi:** Writing – review & editing, Data curation. **Pedro M.M. Soares:** Writing – review & editing, Supervision, Project administration, Conceptualization.

Declaration of competing interest

The authors declare that they have no known competing financial interests or personal relationships that could have appeared to influence the work reported in this paper.

Data availability

Data will be made available on request.

Acknowledgements

The authors would like to acknowledge the financial support of the Portuguese Fundação para a Ciência e a Tecnologia (FCT) I.P./MCTES through national funds (PIDDAC) – UIDB/50019/2020 (https://doi.org/10.54499/UIDB/50019/2020), UIDP/50019/2020 (https://doi.org/10.54499/UIDP/50019/2020), and LA/P/0068/2020 (https://doi.org/10.54499/LA/P/0068/2020). The authors also acknowledge the EEA Financial Mechanism 2014–2021 and the Portuguese Environment Agency through Pre defined Project 2 National Roadmap for Adaptation XXI (PDP 2).

Appendix A. Supplementary data

Supplementary data to this article can be found online at https://doi.org/10.1016/j.oceaneng.2024.117661.

References

Aarnes, O.J., Reistad, M., Breivik, Ø., Bitner-Gregersen, E., Magnusson, A.K., Natvig, B., Vanem, E., 2017. Projected changes in significant wave height toward the end of the 21st century: northeast Atlantic. J. Geophys. Res. Oceans 122, 3394–3403.

Allen-Perkins, S., Calviño, J., Balseiro, C.F., Varela, R.A., Pérez-Muñuzuri, V.Ayensa, Montero, P., 2007. Project RAIA. Towards a North Portugal - Galician oceanographic monitoring network: quality control data. Available online at: https://2007-2020.poctep.eu//sites/default/files/documentos/proyaprob0713/posters_raia_imdis_ing.pdf.

Antunes, C., 2014. Eventos Extremos e a variação do Nível do mar. Actas das 3.as Jornadas de Engenharia Hidrográfica 33–36. https://www.hidrografico.pt/jornada/4.

Antunes, C., Rocha, C., Catita, C., 2019. Coastal flood assessment due to sea level rise and extreme storm events: a case study of the atlantic coast of Portugal's mainland. Geosciences 9 (5), 239. https://doi.org/10.3390/geosciences9050239.

Ardhuin, F., et al., 2010. Semiempirical dissipation source functions for ocean waves. Part I: definition, calibration, and validation. J. Phys. Oceanogr. 40 (9), 1917–1941. https://doi.org/10.1175/2010jpo4324.1.

Athanasiou, P., van Dongeren, A., Giardino, A., et al., 2020. Uncertainties in projections of sandy beach erosion due to sea level rise: an analysis at the European scale. Sci. Rep. 10, 11895 https://doi.org/10.1038/s41598-020-68576-0.

Atkinson, A.L., Baldock, T.L., Birrien, F., Callaghan, D.P., Nielsen, P., Beuzen, T., Turner, I.L., Blenkinsopp, C.E., Ranasinghe, R., 2018. Laboratory investigation of the Bruun Rule and beach response to sea level rise. Coast. Eng. 136, 183–202. https://doi.org/10.1016/j.coastaleng.2018.03.003.

Bernardes, C., Fernández, S., Santos, F., Baptista, P., Silva, P.A., Abreu, T., Coelho, C., Lima, M., Carvalho, R., 2020. Estudo de Viabilidade da Transposição Aluvionar das Barras de Aveiro e da Figueira da Foz. Relatório Intercalar 1. In: Tarefa 1. Análise da Evolução Histórica da Embocadura da Laguna de Aveiro. Universidade de Aveiro/Agência Portuguesa do Ambiente. Portugal. 59pp.

Bidlot, J.-R., Lemos, G., Semedo, A., The C3S Reanalysis Team, ECMWF, 2019. ERA5 reanalysis & ERA5 based ocean wave hindcast. November. In: Presented at the 2nd International Workshop on Waves, Storm Surges and Coastal Hazards, Melbourne, Australia. Retrieved from. http://waveworkshop.org/16thWaves/Presentations/R1%20Wave_Workshop_2019_Bidlot_et_al.pdf.

Booij, N., Ris, R.C., Holthuijsen, L.H., 1999. A third-generation wave model for coastal regains: 1. Model description and validation. J. Geophys. Res. 104 (C4), 7649–7666. https://doi.org/10.1029/98JC02622.

Bruun, P., 1962. Sea-Level rise as cause of shore erosion. American society of civil engineering proceedings. J. Waterw. Harb. Div. 88, 117–130.

Bruun, P., 1988. The Bruun rule of erosion by sea-level rise: a discussion on large-scale two-and three-dimensional usages. J. Coast Res. 4, 627–648.

Cabral, J., 1995. Neotectónica em Portugal continental. In: Ministério da Indústria e Energia, Secretaria de Estado da Indústria, vol. 31. Instituto Geológico e Mineiro.

Camelo, J., Mayo, T.L., Gutmann, E.D., 2020. Projected climate change impacts on hurricane storm surge inundation in the coastal United States. Front. Built Environ. 6, 207pp https://doi.org/10.3389/fbuil.2020.588049.

Camus, P., Losada, I.J., Izaguirre, C., Espejo, A., Menéndez, M., Pérez, J., 2017. Statistical wave climate projections for coastal impact assessments. Earth's Future 5, 918–933. https://doi.org/10.1002/2017EF000609.

Casas-Prat, M., Wang, X.L., Swart, N., 2018. CMIP5-based global wave climate projections including the entire Arctic Ocean. Ocean Model. 123, 66–85.

Church, J.A., et al., 2013. In: Stocker, T.F., et al. (Eds.), *Climate Change 2013*: the Physical Science Basis. IPCC, Cambridge Univ. Press, pp. 1140–1141.

Church, J.A., White, N.J., 2011. Sea-level rise from the late 19th to the early 21st century. Surv. Geophys. 32, 585–602. https://doi.org/10.1007/s10712-011-9119-1.

Coelho, C., Ferreira, M., Silva, P.A., Bernardes, C., Duarte Santos, F., Baptista, P., Lima, M., Carvalho, R., 2021a. Feasibility study of sand bypass at Aveiro and Figueira da Foz bars: Technical Report 2: Task 4, Aveiro. Consortium University of Aveiro and R5 Marine Solutions, 91 pp. (in Portuguese).

Coelho, C., Ferreira, M., Silva, P.A., Bernardes, C., Duarte Santos, F., Baptista, P., Lima, M., Carvalho, R., 2021b. Feasibility study of sand bypass at Aveiro and Figueira da Foz bars: Technical Report 2: Task 4, Figueira da Foz. Consortium University of Aveiro and R5 Marine Solutions, 86 pp. (in Portuguese).

Cooper, J.A.G., Pilkey, O.H., 2004. Sea-level rise and shoreline retreat: time to abandon the Bruun Rule. Global Planet. Change 43 (3–4), 157–171. https://doi.org/10.1016/j.gloplacha.2004.07.001.

D'Anna, M., Idier, D., Castelle, B., Rohmer, J., Cagigal, L., Mendez, F., 2022. Effects of stochastic wave forcing on equilibrium shoreline modelling across the 21st century including Sea-Level rise. Coast. Eng. 175, 1041–1049. https://doi.org/10.1016/j.coastaleng.2022.104149.

D'Anna, M., Idier, D., Castelle, B., Vitousek, S., Le Cozannet, G., 2021. Reinterpreting the Bruun rule in the context of equilibrium shoreline models. J. Mar. Sci. Eng. 9, 974. https://doi.org/10.3390/jmse9090974.

Dee, D.P., et al., 2011. The ERA-Interim reanalysis: configuration and performance of the data assimilation system. Q. J. R. Meteorol. Soc. 137, 1830–1841.

Dobrynin, M., Murawski, J., Baehr, J., Ilyina, T., 2015. Detection and attribution of climate change signal in ocean wind waves. J. Clim. 28 (4), 1578–1591.

Domingues, R.T., Neves de Jesus, S., Ferreira, O., 2021. Place attachment, risk perception, and preparedness in a population exposed to coastal hazards: a case study in Praia de Faro Beach, southern Portugal. Int. J. Disaster Risk Reduc. 60 (2021), 102288 https://doi.org/10.1016/j.ijdrr.2021.102288.

Duarte Santos, F., Mota Lopes, A., Moniz, G., Ramos, L., Taborda, R., 2014. In: Grupo de Trabalho do Litoral: Gestão da Zona Costeira: O desafo da mudança. Filipe Duarte Santos, Gil Penha-Lopes e António Mota Lopes. Lisboa. ISBN: 978-989-99962-1-2.

ECMWF, 2016. IFS documentation CY41R2. https://www.ecmwf.int/node/16651.

Fernández-Fernández, S., Baptista, P., Bernardes, C., Silva, P., Fontán-Bouzas, A., López-Olmedilla, L., Ferreira, C., 2019. Variação da linha de costa em praias arenosas: Aveiro (Portugal). Livro de resumos do IX Congresso sobre Planeamento e Gestão das Zonas Costeiras dos Países de Expressão Portuguesa. Lisboa (Portugal).

Ferreira, A.M., Coelho, C., Narra, P., 2020. Coastal erosion risk assessment to discuss mitigation strategies: barra-Vagueira, Portugal. Nat. Hazards 105, 1069–1107. https://doi.org/10.1007/s11069-020-04349-2.

Feyen, L., Ciscar Martinez, J., Gosling, S., Ibarreta Ruiz, D., Soria Ramirez, A., Dosio, A., Naumann, G., Russo, S., Formetta, G., Forzieri, G., Girardello, M., Spinoni, J., Mentaschi, L., Bisselink, B., Bernhard, J., Gelati, E., Adamovic, M., Guenther, S., De Roo, A., Cammalleri, C., Dottori, F., Bianchi, A., Alfieri, L., Vousdoukas, M., Mongelli, I., Hinkel, J., Ward, P., Gomes Da Costa, H., De Rigo, D., Liberta, G., Durrant, T., San-Miguel-Ayanz, J., Barredo Cano, J., Mauri, A., Caudullo, G., Ceccherini, G., Beck, P., Cescatti, A., Hristov, J., Toreti, A., Perez Dominguez, I., Dentener, F., Fellmann, T., Elleby, C., Ceglar, A., Fumagalli, D., Niemeyer, S., Cerrani, I., Panarello, L., Bratu, M., Després, J., Szewczyk, W., Matei, N., Mulholland, E., Olariaga-Guardiola, M., 2020. Climate Change Impacts and Adaptation in Europe, EUR 30180 EN. Publications Office of the European Union, Luxembourg. ISBN 978-92-76-18123-1. DOI: 10.2760/171121, JRC119178.

Figueiredo, P.M., Cabral, J., Rockwell, T.K., 2014. Recognition of pleistocene marine terraces in the southwest of Portugal (iberian peninsula): evidences of regional quaternary uplift. Ann. Geophys. 56 (6), 5. https://doi.org/10.4401/ag-6276.

French, J., Payo, A., Murray, B., Orford, J., Eliot, M., Cowell, P., 2016. Appropriate complexity for the prediction of coastal and estuarine geomorphic behaviour at decadal to centennial scales. Geomorphology 256, 3–16. https://doi.org/10.1016/j.geomorph.2015.10.005.

Gallagher, S., Gleeson, E., Tiron, R., McGrath, R., Dias, F., 2016. Twenty-first century wave climate projections for Ireland and surface winds in the North Atlantic Ocean. Adv. Sci. Res. 13, 75–80.

Gutiérrez, J.M., Maraun, D., Widmann, M., Huth, R., Hertig, E., Benestad, R., Rössler, O., Wibig, J., Wilcke, R., Kotlarski, S., San Martin, D., 2019. An intercomparison of a large ensemble of statistical downscaling methods over Europe: results from the VALUE perfect predictor cross-validation experiment. Int. J. Climatol. 39 (9), 3750–3785.

Haerter, J.O., Hagemann, S., Moseley, C., Piani, C., 2011. Climate model bias correction and the role of timescales. Hydrol. Earth Syst. Sci. 15, 1065–1079. https://doi.org/10.5194/hess-15-1065-2011.

Hallegatte, S., Green, C., Nicholls, R.J., Corfee-Morlot, J., 2013. Future flood losses in major coastal cities. Nat. Clim. Change 3, 802–806. https://doi.org/10.1038/nclimate1979.

Hay, C.C., Morrow, E., Kopp, R.E., Mitrovica, J.X., 2015. Probabilistic reanalysis of twentieth-century sea-level rise. Nature 517, 481–484. https://doi.org/10.1038/nature14093.

Hersbach, H., Bell, B., Berrisford, P., Hirahara, S., Horányi, A., Muñoz-Sabater, J., Nicolas, J., Peubey, C., Radu, R., Schepers, D., Simmons, A., Soci, C., Abdalla, S., Abellan, X., Balsamo, G., Bechtold, P., Biavati, G., Bidlot, J., Bonavita, M., Chiara, G., Dahlgren, P., Dee, D., Diamantakis, M., Dragani, R., Flemming, J., Forbes, R.,

Fuentes, M., Geer, A., Haimberger, L., Healy, S., Hogan, R., Hólm, E., Janisková, M., Keeley, S., Laloyaux, P., Lopez, P., Lupu, C., Radnoti, G., de Rosnay, P., Rozum, I., Vamborg, F., Villaume, S., Thépaut, J., 2020. The ERA5 global reanalysis. Q. J. R. Meteorol. Soc. 2020, 1–51.

Hinkel, J., Lincke, D., Vafeidis, A.T., Perrette, M., Nicholls, R.J., Tol, R.S.J., Marzeion, B., Fettweis, X., Ionescu, C., Levermann, A., 2014. Coastal flood damage and adaptation costs under 21st century sea-level rise. Proc. Natl. Acad. Sci. U.S.A. 111 (9), 3292–3297. https://doi.org/10.1073/pnas.1222469111.

Howard, T., Palmer, M.D., Bricheno, L.M., 2019. Contributions to 21st century projections of extreme sea-level change around the UK. Environ. Res. Commun. 1 (9), 095002. https://doi.org/10.1088/2515-7620/ab42d7.

Hunt, E., Davidson, M., Steele, E., Amies, J., Scott, T., Russell, P., 2023. Shoreline modelling on timescales of days to decades. Cambridge Prisms: Coastal Futures 1, E16. https://doi.org/10.1017/cft.2023.5.

IHRH, 2003. Case 3: costa da Caparica: artificial sand nourishment with groyne field maintenance. EUrosion Project – Review of experiences of coastal erosion control and management II, 43–60. Report.

IPCC, 2022. In: Pörtner, H.-O., Roberts, D.C., Tignor, M., Poloczanska, E.S., Mintenbeck, K., Alegría, A., Craig, M., Langsdorf, S., Löschke, S., Möller, V., Okem, A., Rama, B. (Eds.), Climate Change 2022: Impacts, Adaptation, and Vulnerability. Contribution of Working Group II to the Sixth Assessment Report of the Intergovernmental Panel on Climate Change. Cambridge University Press. Cambridge University Press, Cambridge, UK and New York, NY, USA, p. 3056. https://doi.org/10.1017/9781009325844.

IPCC, 2014. Climate change 2014: synthesis report. In: Contribution of Working Groups I, II and III to the Fifth Assessment Report of the Intergovernmental Panel on Climate Change. IPCC, Geneva, Switzerland.

Jones, B., O'Neill, B.C., 2016. Spatially explicit global population scenarios consistent with the Shared Socioeconomic Pathways. Environ. Res. Lett. 11, 084003 https://doi.org/10.1088/1748-9326/11/8/084003.

Kamphuis, J.W., 1991. Alongshore sediment transport rate. J. Waterw. Port, Coast. Ocean Eng. 117, 624–640.

Kulp, S.A., Strauss, B.H., 2020. New elevation data triple estimates of global vulnerability to sea-level rise and coastal flooding. Nat. Commun. 10, 4844. https://doi.org/10.1038/s41467-019-12808-z.

Le Cozannet, G., Thiéblemont, R., Rohmer, J., Idier, D., Manceau, J.-C., Quique, R., 2019. Low-end probabilistic Sea-Level projections. Water 11, 1507. https://doi.org/10.3390/w11071507.

Lemos, G., Semedo, A., Dobrynin, M., Behrens, A., Staneva, J., Bidlot, J.-R., Miranda, P., 2019. Mid-twenty-first century global wave climate projections: results from a dynamic CMIP5 based ensemble. Global Planet. Change 172, 69–87.

Lemos, G., Menendez, M., Semedo, A., Camus, P., Hemer, M., Dobrynin, M., Miranda, P., 2020a. On the need of bias correction methods for wave climate projections. Global Planet. Change 186, 103109.

Lemos, G., Semedo, A., Dobrynin, M., Menendez, M., Miranda, P., 2020b. Bias-corrected CMIP5-derived single-forcing future wind-wave climate projections toward the end of the twenty-first century. J. Appl. Meteorol. Climatol. 59 (9), 1393–1414. https://doi.org/10.1175/jamc-d-19-0297.1.

Lemos, G., Semedo, A., Menendez, M., Miranda, P.M.A., Hemer, M., 2021a. On the decreases in North Atlantic significant wave heights from climate projections. Clim. Dynam. https://doi.org/10.1007/s00382-021-05807-8.

Lemos, G., Semedo, A., Hemer, M., Menendez, M., Miranda, P.M.A., 2021b. Remote climate change propagation across the oceans – the directional swell signature. Environ. Res. Lett. https://doi.org/10.1088/1748-9326/ac046b.

Lima, D.C.A., Bento, V.A., Lemos, G., Nogueira, M., Soares, P.M.M., 2023b. A multivariable constrained ensemble of regional climate projections under multi-scenarios for Portugal – Part II: sectoral climate indices. Climate Services 30 (100377). https://doi.org/10.1016/j.cliser.2023.100377.

Lima, D.C.A., Lemos, G., Bento, V.A., Nogueira, M., Soares, P.M.M., 2023a. A multivariable constrained ensemble of regional climate projections under multi-scenarios for Portugal – Part I: an overview of impacts on means and extremes. Climate Services 30 (100351). https://doi.org/10.1016/j.cliser.2023.100351.

Lira, C.P., Nobre Silva, A., Taborda, R., Freire de Andrade, C., 2016. Coastline evolution of Portuguese low-lying sandy coast in the last 50 years: an integrated approach. Earth Syst. Sci. Data 8, 265–278. https://doi.org/10.5194/essd-8-265-2016.

Luijendijk, A., Hagenaars, G., Ranasinghe, R., et al., 2018. The state of the world's beaches. Sci. Rep. 8, 6641. https://doi.org/10.1038/s41598-018-24630-6.

Lyon, C., Saupe, E., Smith, C., Hill, D., Beckerman, A., Stringer, L., Marchant, R., McKay, J., Burke, A., O'Higgins, P., Dunhill, A., Allen, B., Riel-Salvatore, J., Aze, T., 2022. Climate change research and action must look beyond 2100. Global Change Biol. 28, 349–361.

Maraun, D., Shepherd, T.G., Widmann, M., Zappa, G., Walton, D., Gutiérrez, J.M., Hagemann, S., Richter, I., Soares, P.M., Hall, A., Mearns, L.O., 2017. Towards process-informed bias correction of climate change simulations. Nat. Clim. Change 7 (11), 764–773.

Maraun, D., Huth, R., Gutiérrez, J.M., Martín, D.S., Dubrovsky, M., Fischer, A., Hertig, E., Soares, P.M.M., Bartholy, J., Pongrácz, R., Widmann, M., 2019. The VALUE perfect predictor experiment: evaluation of temporal variability. Int. J. Climatol. 39 (9), 3786–3818.

McGranahan, G., Balk, D., Anderson, B., 2007. The rising tide: assessing the risks of climate change and human settlements in low elevation coastal zones. Environ. Urbanization 19 (1), 17–37. https://doi.org/10.1177/0956247807076960.

Mentaschi, L., Vousdoukas, M.I., Voukouvalas, E., Dosio, A., Feyen, L., 2017. Global changes of extreme coastal wave energy fluxes triggered by intensified teleconnection patterns. Geophys. Res. Lett. 44, 2416–2426. https://doi.org/10.1002/2016GL072488.

Mentaschi, L., Vousdoukas, M.I., Pekel, J.-F., Voukouvalas, E., Feyen, L., 2018. Global long-term observations of coastal erosion and accretion. Sci. Rep. 8 (1), 12876.

Montaño, J., Coco, G., Antolínez, J.A.A., et al., 2020. Blind testing of shoreline evolution models. Sci. Rep. 10, 2137. https://doi.org/10.1038/s41598-020-59018-y.

Morim, J., Hemer, M.A., Cartwright, N., Strauss, D., Andutta, F., 2018. On the concordance of 21st century wind-wave climate projections. Global Planet. Change 167, 160–171.

Morim, J., Hemer, M.A., Wang, X., Cartwright, N., Trenham, C., Semedo, A., Young, I., Bricheno, L., Camus, P., Casas-Prat, M., Erikson, L., Mentaschi, L., Mori, N., Shimura, T., Timmermans, B., Aarnes, O., Breivik, Ø., Behrens, A., Dobrynin, M., Menendez, M., Staneva, J., Wehner, M., Wolf, J., Kamranzad, B., Webb, A., Stopa, J., Andutta, F., 2019. Robustness and uncertainties in global multivariate wind-wave climate projections. Nat. Clim. Change 9, 711–718.

Nerem, R.S., Chambers, D.P., Choe, C., Mitchum, G.T., 2010. Estimating mean sea level change from the TOPEX and jason altimeter missions. Mar. Geodesy 33, 435–446. https://doi.org/10.1080/01490419.2010.491031.

Neumann, B., Vafeidis, A.T., Zimmermann, J., Nicholls, R.J., 2015. Future coastal population growth and exposure to Sea-Level rise and coastal flooding - a global assessment. PLoS One 10 (3), e0118571. https://doi.org/10.1371/journal.pone.0118571.

Nunes, A.J., Cordeiro, M.F.N., 2013. Alteração da linha de costa entre a Figueira da Foz e S. Pedro de Moel após o prolongamento do molhe norte do Mondego. Actas do VI Congresso Nacional de Geomorfologia, Coimbra, pp. 6–10.

Oliveira, F.S.B.F., Brito, F.A., 2015. Evolução da morfologia costeira a sul da embocadura do rio Mondego, de 1975 a 2011. In: VIII Congresso sobre Planeamento e Gestão das Zonas Costeiras dos Países de Expressão Portuguesa. Universidade de Aveiro, Aveiro, p. 15.

Pelnard-Considere, R., 1956. Essai de Theorie de L'evolution des Formes de Rivage en Plages de Sable et de Galets. Les Energies de la Mer: Compte Rendu Des Quatriemes Journees de L'hydraulique, Paris 13, 14 and 15 Juin 1956, Question III, rapport 1, 74, 1-10.

Pinto, C.A., Silveira, T.M., Taborda, R., 2015. Alimentação artificial das praias da Costa da Caparica: síntese dos resultados de monitorização (2007 a 2014). In: 3ª Conferencia sobre morfodinâmica estuarina e costeira. Universidade do Algarve, 14-15 May 2015. Praia de Faro.

Perez, J., Menéndez, M., Camus, P., Méndez, F.J., Losada, I.J., 2015. Statistical multi-model climate projections of surface ocean waves in Europe. Ocean Modell. 96, 161–170. https://doi.org/10.1016/j.ocemod.2015.06.001.

Pinto, C.A., 2016. Coastal erosion and sediment management in Portugal. In: Proceedings of the CEDA Iberian Conference—Dredging for Sustainable Port Development, Lisbon, Portugal.

Pinto, C.A., Silveira, T.M., Teixeira, S.B., 2020. Beach nourishment practice in mainland Portugal (1950–2017): overview and retrospective. Ocean Coast Manag. 192, 105211.

Pinto, C.A., Taborda, R., Andrade, C., 2007. Evolução recente da linha de costa no troço Cova do Vapor – S. João da Caparica. In: 5as Jornadas Portuguesas de Engenharia Costeira e Portuária, Lisboa. PIANC. AIPCN, Lisboa, p. 13.

Pinto, C., Taborda, R., Andrade, C., Baptista, P., Silva, P., Alves, Mendes, D., Pais-Barbosa, J., 2022. Morphological development and behaviour of a shoreface nourishment in the Portuguese western coast. J. Mar. Sci. Eng. 10 (2), 146. https://doi.org/10.3390/jmse10020146.

Ranasinghe, R., Callaghan, D., Stive, M.J.F., 2012. Estimating coastal recession due to sea level rise: beyond the Bruun rule. Climatic Change 110 (3–4), 561–574. https://doi.org/10.1007/s10584-011-0107-8.

Ranasinghe, R., 2016. Assessing climate change impacts on open sandy coasts: a review. Earth Sci. Rev. 160, 320–332.

Ranasinghe, R., 2020. On the need for a new generation of coastal change models for the 21st century. Sci. Rep. 10, 1. https://doi.org/10.1038/s41598-020-58376-x.

Rascle, N., Ardhuin, F., 2013. A global wave parameter database for geophysical applications. Part 2: model validation with improved source term parameterization. Ocean Model. 70, 174–188. https://doi.org/10.1016/j.ocemod.2012.12.001.

Reimann, L., Vafeidis, A., Honsel, L., 2023. Population development as a driver of coastal risk: current trends and future pathways. Cambridge Prisms: Coastal Futures 1, E14. https://doi.org/10.1017/cft.2023.3.

Rentschler, J., Avner, P., Marconcini, M., Su, R., Strano, E., Vousdoukas, M., Hallegatte, S., 2023. Global evidence of rapid urban growth in flood zones since 1985. Nature 622, 87–92. https://doi.org/10.1038/s41586-023-06468-9.

Riahi, K., Rao, S., Krey, V., Cho, C., Chirkov, V., Fischer, G., Kindermann, G., Nakicenovic, N., Rafaj, P., 2011. Rcp 8.5 – a scenario of comparatively high greenhouse gas emissions. Climatic Change 109, 33–57. https://doi.org/10.1007/s10584-011-0149-y.

Ritphring, S., Somphong, C., Udo, K., Kazama, S., 2018. Projections of future beach loss due to sea level rise for sandy beaches along Thailand's coastlines. J. Coast Res. 85 (1), 541–545. https://doi.org/10.2112/SI85-109.1.

Rocha, C., Antunes, C., Catita, C., 2020. Coastal vulnerability assessment due to sea level rise: the case study of the atlantic coast of mainland Portugal. Water 12 (2), 360. https://doi.org/10.3390/w12020360.

Rocheta, E., Evans, J.P., Sharma, A., 2017. Can bias correction of regional climate model lateral boundary conditions improve low-frequencyrainfall variability? J. Clim. 30, 9785–9806.

Roelvink, D., 2011. A Guide to Modeling Coastal Morphology 12.

Roelvink, J.A., Huisman, B., Elghandour, A., Ghonim, M., Reyns, J., 2020. Efficient modeling of complex sandy coastal evolution at monthly to century time scales. Front. Mar. Sci. 7, 535.

Semedo, A., Sušelj, K., Rutgersson, A., Sterl, A., 2011. A global view on the wind sea and swell climate and variability from EERA-40. J. Clim. 24 (5), 1461–1479.

Senechal, N., Coco, G., Bryan, K.R., Holman, R.A., 2011. Wave run-up during extreme storm conditions. J. Geophys. Res.: Oceans 116 (C7).
Sherwood, C.R., Dongeren, A.V., Doyle, J., Hegermiller, C.A., Hsu, T.-J., Karla, T.S., Olabarrieta, M., Penko, A.M., Rafati, Y., Roelvink, D., Lugt, M.V.D., Veeramony, J., Warner, J.C., 2022. Modeling the morphodynamics of coastal responses to extreme events: what shape are we in? Ann. Rev. Mar. Sci 14, 457–492.
Soares, P.M.M., Maraun, D., Brands, S., Jury, M.W., Gutiérrez, J.M., San-Martín, D., Hertig, E., Huth, R., Belušić Vozila, A., Cardoso, R.M., Kotlarski, S., 2019. Process-based evaluation of the VALUE perfect predictor experiment of statistical downscaling methods. Int. J. Climatol. 39 (9), 3868–3893.
Soares, P.M.M., Lima, D.C.A., 2022. Water scarcity down to earth surface in a Mediterranean climate: the extreme future of soil moisture in Portugal. J. Hydrol. 615 B (128731) https://doi.org/10.1016/j.jhydrol.2022.128731.
Soares, P.M.M., Lemos, G., Lima, D.C.A., 2023a. Critical analysis of CMIPs past climate model projections in a regional context: the iberian climate. Int. J. Climatol. https://doi.org/10.1002/joc.7973.
Soares, P.M.M., Careto, J.A.M., Russo, A., Lima, D.C.A., 2023b. The future of Iberian droughts: a deeper analysis based on multi-scenario and a new multi-model ensemble approach. Nat. Hazards 117, 2001–2028. https://doi.org/10.1007/s11069-023-05938-7.
Storlazzi, C., Gingerich, S.B., Dongeren, A., Cheriton, O., Swarzenski, P., Quataert, E., Voss, C., Field, D., Annamalai, H., Piniak, G., McCall, R., 2018. Most atolls will be uninhabitable by the mid-21st century because of sea-level rise exacerbating wave-driven flooding. Sci. Adv. 4 (4) https://doi.org/10.1126/sciadv.aap9741.
Studholme, J., Fedorov, A.V., Gulev, S.K., Emanuel, K., Hodges, K., 2022. Poleward expansion of tropical cyclone latitudes in warming climates. Nat. Geosci. 15, 14–28.
Sweet, W.V., Kopp, R.E., Weaver, C.P., Obeysekera, J., Horton, R.M., Thieler, E.R., Zervas, C., 2017. Global and regional sea level rise scenarios for the United States. In: NOAA Technical Report. NOAA, Silver Spring, MD, USA. NOS CO-OPS 083.
Sweet, W.V., Hamlington, B.D., Kopp, R.E., Weaver, C.P., Barnard, P.L., Bekaert, D., Brooks, W., Craghan, M., Dusek, G., Frederikse, T., Garner, G., Genz, A.S., Krasting, J.P., Larour, E., Marcy, D., Marra, J.J., Obeysekera, J., Osler, M., Pendleton, M., Roman, D., Schmied, L., Veatch, W., White, K.D., Zuzak, C., 2022. Global and Regional Sea Level Rise Scenarios for the United States: Updated Mean Projections and Extreme Water Level Probabilities along U.S. Coastlines. National Oceanic and Atmospheric Administration, National Ocean Service, Silver Spring, MD, p. 111. NOAA Technical Report NOS 01. https://oceanservice.noaa.gov/hazards/sealevelrise/noaa-nostechrpt01-global-regional-SLR-scenarios-US.pdf.
Toimil, A., Camus, P., Losada, I.J., Le Cozannet, G., Nicholls, R.J., Idier, D., Maspataud, A., 2020. Climate change-driven coastal erosion modelling in temperate sandy beaches: methods and uncertainty treatment. Earth Sci. Rev. 202, 103110 https://doi.org/10.1016/j.earscirev.2020.103110.
Tolman, H.L., 2002. User Manual and System Documentation of WAVEWATCH-III Version 2.22. *Tech. Report 222*. NOAA/NWS/NCEP/MMAB.
U. S. Army Corps of Engineers, 1984. Shore Protection Manual. U. S. Army Corps of Engineers, Coastal Engineering Research Center, Dept. of the Army, Vicksburg, Mississippi.
Udo, K., Takeda, Y., 2017. Projections of future beach loss in Japan due to Sea-Level rise and uncertainties in projected beach loss. Coast Eng. J. 59 (2), 1740006 https://doi.org/10.1142/S057856341740006X.
Veloso-Gomes, F., Taveira-Pinto, F., Neves, L., 2004. Esposende – Ofir Stretch – Case Study. Coastal Practice Network. Project part-funded by the European Union.
Veloso-Gomes, F., Costa, J., Rodrigues, A., Taveira Pinto, F., Barbosa, J.P., Neves, L., 2009. Costa da Caparica artificial sand nourishment and coastal dynamics. J. Coast. Res. Spec. 56, 678–682.
Vicente, C., Clímaco, M., 2015. Evolução da costa do Douro ao Cabo Mondego. Proposta de uma metodologia de estudo, 34. Technical Report, LNEC, Lisbon, Portugal.
Vitousek, S., Vos, K., Splinter, K.D., Erikson, L., Barnard, P.L., 2023. A model integrating satellite-derived shoreline observations for predicting fine-scale shoreline response to waves and Sea-Level rise across large coastal regions. J. Geophys. Res.: Earth Surf. 128 (7), e2022JF006936 https://doi.org/10.1029/2022JF006936.
Vousdoukas, M.I., Mentaschi, L., Voukouvalas, E., Verlaan, M., Feyen, L., 2017. Extreme sea levels on the rise along Europe's coasts. Earth's Future 5 (3), 304–323.
Vousdoukas, M.I., Ranasinghe, R., Mentaschi, L., Plomaritis, T.A., Athanasiou, P., Luijendijk, A., Feyen, L., 2020. Sandy coastlines under threat of erosion. Nat. Clim. Change 10, 260–263. https://doi.org/10.1038/s41558-020-0697-0.
Wang, J., Wang, Y., 2022. Evaluation of the ERA5 significant wave height against NDBC buoy data from 1979 to 2019. Mar. Geodesy 45, 151–165. https://doi.org/10.1080/01490419.2021.2011502.
Webb, A., Shimura, T., Mori, N., 2018. A high-resolution future wave climate projection for the coastal northwestern atlantic. The 65th Coast. Eng. Lectures 74 (2).
Zhang, K., Douglas, B.C., Leatherman, S.P., 2004. Global warming and coastal erosion. Clim. Change 64, 41–58.